

**SURFACE WRINKLING BASED METHOD OF MEASURING THIN FILM'S  
MECHANICAL PROPERTIES**

by

**Jiani Niu**

B.S. in Textile and Dying Engineering, Donghua University, 2008

Submitted to the Graduate Faculty of  
Swanson School of Engineering in partial fulfillment  
of the requirements for the degree of  
Master of Science

University of Pittsburgh

2012

UNIVERSITY OF PITTSBURGH  
SWANSON SCHOOL OF ENGINEERING

This thesis was presented

by

Jiani Niu

It was defended on

July 23, 2012

and approved by

Sachin Velankar, PhD, Associate Professor, Department of Chemical and Petroleum  
Engineering

Götz Veser , PhD, Professor, Department of Chemical and Petroleum Engineering

Lei Li, PhD, Assistant Professor, Department of Chemical and Petroleum Engineering

Thesis Advisor: Sachin Velankar, PhD, Associate Professor, Department of Chemical and  
Petroleum Engineering

Copyright © by Jiani Niu

2012

# **SURFACE WRINKLING BASED METHOD OF MEASURING THIN FILM'S MECHANICAL PROPERTIES**

Jiani Niu, M.S.

University of Pittsburgh, 2012

The main goal of this project is to develop a wrinkling-based method to measure mechanical properties of thin interfacial polymeric films. Instead of working on a mechanically equilibrium system, this study is focused on the case where mechanical equilibrium is difficult to reach due to the very high viscosity of the bulk phases. This situation is appropriate when considering films formed at the interface between molten immiscible homopolymers.

This thesis describes an air/viscous polymer system with a few-micron scale thick polymer film placed at the interface. We have developed a method to generate dynamic wrinkle patterns on the film via compressing the high viscous substrate. Two experiment parameters are controlled: the liquid substrate thickness  $H$  and the compressing strain rate  $\dot{\epsilon}$ . This thesis developed an accurate method to measure  $H$  while avoiding the interference from the edge effect of the fluid. Other parameters such as strain rate, wrinkling wavelength and critical strain were all calculated from video analysis using Matlab.

We report on the wave number of wrinkles and the critical strain for wrinkling as a function of compression strain rate and of the liquid substrate thickness. Critical strains under different compression strain rate and substrate thickness have been obtained via analyzing the strain for the onset wrinkle. The experiments suggest that the film experiences stresses that are far higher than can be explained by simple models of the fluid mechanics of the deformation.

## TABLE OF CONTENTS

<b>PREFACE.....</b>	<b>XI</b>
<b>1.0 INTRODUCTION.....</b>	<b>1</b>
<b>2.0 LITERATURE REVIEW.....</b>	<b>3</b>
<b>2.1 BACKGROUND .....</b>	<b>3</b>
<b>2.2 APPLICATION OF SURFACE WRINKLING .....</b>	<b>3</b>
<b>2.2.1 Measurement on solid films with a solid substrate .....</b>	<b>3</b>
<b>2.2.2 Measurement on films with a liquid substrate .....</b>	<b>7</b>
<b>2.2.3 Other buckling based measurements .....</b>	<b>11</b>
<b>2.2.4 Research on films coupled with viscous substrate .....</b>	<b>12</b>
<b>3.0 MATERIALS AND METHODS .....</b>	<b>16</b>
<b>3.1 EXPERIMENT DESIGN.....</b>	<b>17</b>
<b>3.2 MANUFACTURE OF RUBBER TRAY.....</b>	<b>21</b>
<b>3.3 DATA MANAGEMENT AND IMAGE CAPTURE.....</b>	<b>22</b>
<b>3.4 MATERIALS .....</b>	<b>23</b>
<b>4.0 RESULTS AND DISCUSSION .....</b>	<b>24</b>
<b>4.1 EXPERIMENTAL PROCEDURE .....</b>	<b>24</b>
<b>4.1.1 Method of measuring substrate thickness .....</b>	<b>25</b>
<b>4.1.2 Method of obtaining wrinkle wavelength from image.....</b>	<b>27</b>

4.1.3	Strain rate calculation .....	29
4.2	VALIDATION EXPERIMENTS .....	30
4.3	RESULTS .....	34
4.3.1	Wavelength versus strain rate .....	34
4.3.2	Wavelength versus viscous layer thickness.....	35
4.3.3	Critical strain versus strain rate.....	37
4.3.4	Critical strain versus substrate thickness .....	38
4.4	DISCUSSION.....	39
4.4.1	Data normalization .....	39
4.4.2	Comparison with theory for films with prestress .....	42
4.4.3	Deriving film stress .....	44
4.4.4	Relation with strain rate and thickness .....	47
5.0	CONCLUSION AND FUTURE WORK .....	60
5.1	CONCLUSION .....	60
5.2	FUTURE WORK.....	61
APPENDIX A .....		62
A.1	SELECTING REACTANTS .....	63
A.2	CALCULATING AMOUNTS OF REACTANTS.....	64
A.3	FILM SYNTHESIS .....	65
A.4	EXPERIMENTAL METHODS .....	65
A.5	RESULTS .....	67
BIBLIOGRAPHY .....		70

## LIST OF TABLES

Table 1	Typical properties of the P-10 silicone. ....	21
Table 2	Typical properties of LIR-50. ....	23
Table 3	Parameters in the experiment. ....	39
Table 4	Logarithm of normalized wrinkle number versus logarithm of normalized strain. ....	51
Table 5	Fitted normalized wrinkle number versus normalized strain rate, slope fixed to $\frac{1}{3}$ . ..	52
Table 6	Fitted normalized wrinkle number versus normalized strain rate, slope fixed to $\frac{1}{2}$ . ..	57
Table 7	Properties of the reactant selected for synthesizing polymeric film. ....	64

## LIST OF FIGURES

Figure 1	Geometry for inducing wrinkles in thin films attached to soft elastic substrates by compressing the substrate. ....	4
Figure 2	Modulus and wrinkle wavelength versus thickness for a flow-coated thickness gradient sample. (Stafford et al, [2]). Figure used with permission.....	5
Figure 3	Schematics of Huang’s Experiment. ....	8
Figure 4	Verification of Huang’s Experiment(Huang et al, [25]). ....	10
Figure 5	AFM image of buckled SiGe film on BPSG after 800°C, 90 min annealing. ....	13
Figure 6	Normalized growth rate with respect to the normalized wave number. ....	14
Figure 7	Schematic of the flat and the wrinkled states of a polymeric film on a highly viscous layer. ....	17
Figure 8	The general experiment system design. ....	19
Figure 9	A photograph and a schematic sketch of the Instron tensile testing machine. ....	19
Figure 10	The rail-carriage assembly. ....	20
Figure 11	The silicone rubber tray. ....	20
Figure 12	Setup of the recording devices. ....	22
Figure 13	Placement of a film on the liquid substrate. ....	24
Figure 14	Measurements with the micrometer. ....	26
Figure 15	The contact between the lens and the surface. ....	26
Figure 16	Schematic of the video recording region. ....	27
Figure 17	Schematic of the markers movements.....	29
Figure 18	Video frames illustrating the displacement of the markers.....	30



Figure 19	Marker displacements versus positions after 0.17s.....	31
Figure 20	Strain versus time during the whole releasing process. Instron velocity: 100 mm/min. .....	32
Figure 21	Strain versus time during the whole releasing process. Instron velocity: 300 mm/min. .....	32
Figure 22	Strain versus time during the whole releasing process. Instron velocity: 500 mm/min. .....	33
Figure 23	Instron velocity versus calculated strain rate. ....	34
Figure 24	Wavelength verses strain rate. Thickness: 2.7mm.....	35
Figure 25	Wavelength verses strain rate. Thickness[mm] varies. ....	36
Figure 26	Critical strain verses strain rate. Thickness: 2.7mm. ....	37
Figure 27	Critical strain verses strain rate. Thickness [mm] varies. ....	38
Figure 28	Wrinkle number versus strain rate. Thickness ratio varies. ....	40
Figure 29	Normalized wrinkle number versus normalized strain rate. Thickness ratio varies. ..	40
Figure 30	Normalized wrinkle number versus normalized strain rate for two different viscous substrates .....	41
Figure 31	Normalized wrinkle number $kH$ versus normalized strain rate. ....	41
Figure 32	Normalized wrinkle growth rate versus normalized wrinkle number according to Huang's theory. ....	42
Figure 33	Fastest growing wave number versus thickness ratio according to Huang and Suo .add citation.....	43
Figure 34	Measured normalized wrinkle number versus thickness ratio. ....	44
Figure 35	Normalized growth rate versus normalized wrinkle number in the limit of thickness ratio $H/h \rightarrow \infty$ . The pre-strain varies. ....	45
Figure 36	Pre-strain versus normalized fastest growing wave number, when thickness ratio $H/h \rightarrow \infty$ . ....	46
Figure 37	Stress [Pa] on the film versus strain rate $\dot{\epsilon}$ [ $s^{-1}$ ] for different thickness ratio.....	47
Figure 38	Ratio of film length to wavelength $L/\lambda$ . The normalized strain rate varies. ....	48

Figure 39	Logarithm of normalized wrinkle number versus logarithm of normalized strain rate. .....	50
Figure 40	Fitted normalized wrinkle number versus normalized strain rate, with their correspondently fitting line that fixed the slope to $\frac{1}{3}$ .....	52
Figure 41	Intercept versus logarithm of thickness ratio. ....	53
Figure 42	An example of obtaining error bar of a single thickness ratio for figure 41 .....	54
Figure 43	Velocity profile in the substrate prior to buckling. ....	55
Figure 44	Fitted normalized wrinkle number versus normalized strain rate, slope fixed to $\frac{1}{2}$ , with their correspondently fitting line that fixed the slope to $\frac{1}{3}$ . ....	57
Figure 45	Intercept versus log nature of thickness ratio.....	58
Figure 46	Stress versus normalized strain rate under different substrate thickness .....	59
Figure 47	Setup of the poking experiment. ....	66
Figure 48	Wrinkles induction on the interfacial film. ....	67
Figure 49	Images of spherical formations near the film surface. ....	68
Figure 50	Images of film surface.....	69

## **PREFACE**

First and foremost, I would like to express my sincere appreciation to my research advisor Dr. Sachin Velankar, for his patience, guidance and great support for my research and graduate study. He provided me with the opportunities to learn lots of new techniques and new experiences.

I appreciate the help from Dr. Sourav Chatterji who provided the Matlab program for analyzing the experiment result more efficiently.

I am gratefully for the encouragement and unfailing support from FengYu.

All my fellow lab mate, they helped me to become familiar with the lab, inspired me with new ideas for my research. It was really great to work with them.

I would also like to thank all my families and friends, who supported me such long time for my life, my study and my research. They witness my growth, and supported me all my failures and successes.

## **1.0 INTRODUCTION**

When immiscible polymers are blended, a compatibilizer is often formed by an interfacial coupling reaction between two reactive molecules that are initially mixed into the immiscible phases. Generally these compatibilizer films are thin and solid like as a result of its crosslink structures formed in polymerization. However, their mechanical properties are difficult to measure since they are molecularly thin and cannot be made free-standing. The goal of this project is to develop a method that can measure the mechanical properties of the thin polymeric films formed between immiscible phases. In this thesis, wrinkling based measurement has been considered.

Wrinkling refers to the appearance of sinusoidal waves on an initially flat surface. The scale of wrinkling spans a huge range, from thousands meters to nanometers. For example, mountains are a form of wrinkle generate by the compression of the earth crust. The ripple of the milk skin on the surface of boiled milk is another kind of wrinkle. When a fruit dries, the pulp contracts by losing water, whereas the skin does not shrink significantly which result in wrinkle formation[1] As the development of experiment technology, versatile methods of producing controlled wrinkling pattern have been established, and the study of wrinkling pattern and its application in various research areas are receiving extensive attention.

One application we are interested in is characterizing mechanical properties of Nano-thin films that are widely used in electronic devices. The previous research is mainly focused on films placed on a solid supporting substrate after it has been manufactured, and in this case, the film's mechanical properties can be related to the wrinkle characteristics[2-6] In our case however (1) the film will be generated in the interfacial between two immiscible bulk phases and could not be taken out easily. (2) The substrates in contact with the film are highly viscous polymeric materials. Accordingly, the previously developed method using solid substrates cannot be applied here. Therefore a new experiment method will be developed to relate wrinkling pattern and film mechanics accurately.

In this thesis, we study the controlled surface wrinkling of a film with thickness in the micron meter scale on a highly viscous substrate. The relations between the wavelength of wrinkle, and 1) the compressing speed and 2) the thickness of the substrate; the critical strain applied to generate the wrinkle pattern and 1) the compressing speed and 2) the thickness of the substrate have been established.

Chapter 2 is a literature review on the previous relevant works, consisting of methods used in the production of surface wrinkling on films coupled with different substrate as well as the application of the wrinkle based measurement in metrology. Chapter 3 describes the design of the experiment including materials, methods used in this project. The result and discussion of wrinkling on the film coupled with a high viscous liquid substrate has been carried out in Chapter 4. Chapter 5 is the conclusions and suggestions for future work. Appendix A is about generating an interfacial thin-polymeric film via polymerization of two immiscible polymer bulks.

## **2.0 LITERATURE REVIEW**

### **2.1 BACKGROUND**

The history of studying elastic instability phenomena can be traced back to the 18th century. Euler first studied buckling phenomena in columns and discovered a relationship between the critical load required for buckling and the stiffness and geometry of the columns [7]. After that, more attention has been paid to the area of buckling phenomena, and several related theories have been developed for example, the plate buckling theory and shell buckling theory[8]. Recently numerous studies of thin film buckling have been conducted [5, 9-15]. Wrinkling-based measurement for mechanical properties of thin film is one application that is receiving more attention due to its lower cost comparing to other methods [2, 16-20].

### **2.2 APPLICATION OF SURFACE WRINKLING**

#### **2.2.1 Measurement on solid films with a solid substrate**

Stafford and coworkers developed a method called strain-induced elastic buckling instability for mechanical measurements (SIEBIMM) using the wrinkling phenomenon on nanometer thickness

films to get the modulus of the skin material. [2] Figure 1 schematically showing the process of induce wrinkle on the surface of film.

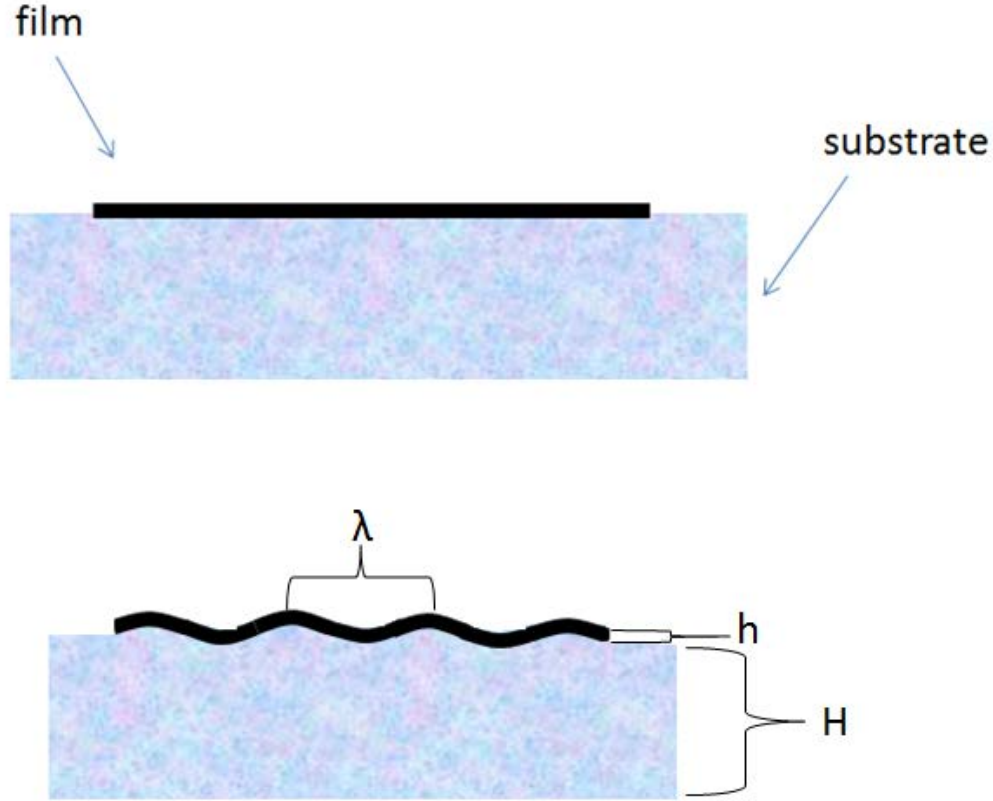


**Figure 1** Geometry for inducing wrinkles in thin films attached to soft elastic substrates by compressing the substrate.

In Figure 1, a thin film has been placed on a soft substrate. Wrinkles have been generated by compressing the substrate. The various relevant properties are:  $\lambda$  is the wavelength of wrinkle;  $H$  is the thickness of substrate,  $h$  is the thickness of film  $E_s$  is the modulus of substrate,  $E_f$  is the modulus of film,  $\nu_f$  is the Poisson ratio of the film,  $\nu_s$  is the Poisson ratio of the substrate.

The total elastic energy of the system of thin film coupled with substrate is  $U=U_b+U_e$  where  $U_b$  is the bending energy of the film and  $U_e$  is the elastic energy of the substrate. Via minimizing the total energy of the system, a critical wavelength can be obtained. [21]

$$\lambda_c = 2\pi h \left[ \frac{(1 - \nu_s^2)E_f}{3(1 - \nu_f^2)E_s} \right]^{1/3} \quad (1)$$

The above equation can be rearranged to calculate the modulus of the film.

$$E_f = 3(1 - \nu_f^2) \frac{E_s}{(1 - \nu_s^2)} \left[ \frac{\lambda}{2\pi h} \right]^3 \quad (2)$$

Thus, if wavelength is measured, then, with knowledge of the film thickness and substrate modulus, the modulus of the film can be calculated. Stafford et.al conducted experiments to test this method to measure film properties.[2] the result is present in Figure 2.

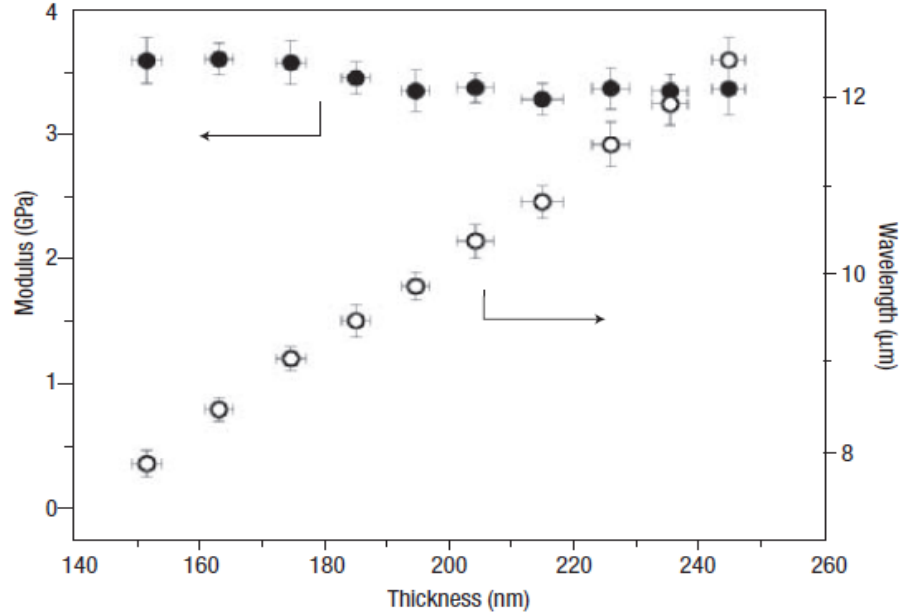


**Figure 2 Modulus and wrinkle wavelength versus thickness for a flow-coated thickness gradient sample. (Stafford et al, [2]). Figure used with permission.**

Samples with a gradient in film thickness were prepared by flow coating polystyrene on silicon wafer and then transferring it to the surface of PDMS rubber. The rubber was then compressed to induce wrinkles. The linear increase in wrinkling wavelength (the open circles) with film thickness is consistent with equation (1) With the known quantities of film wavelength



and thickness, equation (2) was used to calculate the substrate modulus, and the calculated value (3.5 GPa) had good agreement with the reported bulk values.

Additional validation experiments were carried out by Stafford et al [2] by measuring the modulus of plasticized films. Once again, the dependence of modulus on plasticizer content obtained from equation (2) agreed well with independent measurements with nanoindentation. Similarly good agreement was obtained for low-k dielectric films with various levels of porosity.

A related experiment has been carried out by the same group. They grafted poly(2-hydroxyethyl methacrylate) polymer brush layer on an PDMS substrate. By assuming the Poisson ratio is the same for the polymer brush and the substrate, the equation (1) could be modified as follows:

$$h = \frac{\lambda}{2\pi} \left( \frac{3E_s}{E_f} \right)^{1/3} \quad (3)$$

In this case, assuming that the moduli of the film and the substrate are equal to their bulk values and by measuring the wrinkle wavelength, the thickness of the film could be calculated. This offers a simple method of measuring the thickness of grafted polymer brush layers.

In conclusion, with SIEBIMM method, either the modulus or the thickness of the film could be calculated if the other parameters present in equation (1) are known.

Before finishing this section, we must note several conditions that must be met for applying equations 1-3. (a) low strain ( $\epsilon \ll 10\%$ ), (b)  $E_f/E_s \gg 1$ , (c) the substrate being much thicker than the film, (d) the amplitude of the buckles is much smaller than their wavelength and (e) the deformation of the film is fully elastic.

### 2.2.2 Measurement on films with a liquid substrate

M.A.Biot first studied the wrinkling instability of a layered viscoelastic medium under compression[22]. in the 90<sup>th</sup>, L.Bourdieu and his coworker discovered the buckling behavior on a polymerized monomolecular films which is in lying on water via compressing the film[23].

Recently Pocivavsek et al did the analysis on the wrinkle pattern generate by unidirectional compressing a film lying on top of water[24]. The energy in the system contains two parts:  $U=U_b+U_k$  in this case  $U_b$  is the bending energy of this film in this case given by

$$U_b \sim BL \left( \frac{A}{\lambda^2} \right)^2 \quad (4)$$

Where B is the bending stiffness of the surface given by as  $B=Eh^3/12(1-\nu^2)$ . L is the length of the film. A is the amplitude of the wrinkle and  $\lambda$  is the wavelength of the wrinkle and  $U_k$  is the gravitational potential energy for the substrate which gives:

$$U_k \sim KLA^2 \quad (5)$$

K is the stiffness of the substrate and for a fluid  $K = \rho g$ , where  $\rho$  is the fluid density and g is the acceleration due to gravity. By balance the bending energy from the film and the elastic energy from the substrate and fit with experiment data they obtained:

$$\lambda = 2\pi \left( \frac{B}{K} \right)^{1/4} \quad (6)$$

Equation 6 could be also rewritten as:

$$\lambda = 2\pi \left[ \frac{E}{12(1-\nu^2)\rho g} \right]^{1/4} h^{3/4} \quad (7)$$

In the above case, the film was compressed in a unidirectional fashion. Huang et al [25] used a different approach of applying a radially inward force on a floating film. This gives rise to a biaxial compression and hence radial wrinkles. Figure 3 schematically shows the procedure of introducing radial wrinkles on the film surface. The radial wrinkle in this case has finite length due to the tension at the edge.

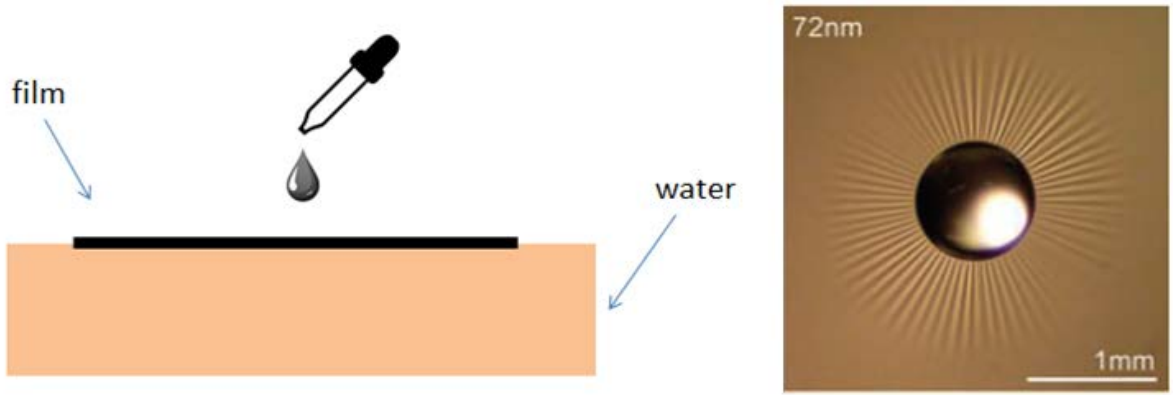


**Figure 3 Schematics of Huang's Experiment.**

**Left:** A droplet is placed in the center of a floating film. **Right:** image of the radial wrinkle induced by this method.

The radial wrinkles had a finite length due to the surface tension from the edge of the film. Thus two independent quantities could be collected from the radial wrinkle pattern: the number of wrinkles (which is related to the wavelength of wrinkles) and the length of a single wrinkle. By adapting previous results from Cerda to a radial geometry [26, 27] the wavelength could be computed as:

$$\lambda \sim \left( \frac{B}{\sigma_{rr}} \right)^{1/4} r^{1/2} \quad (8)$$

Where B is the bending stiffness of the surface given by as  $B = Eh^3/12(1-\nu^2)$ , and  $\sigma_{rr}$  is the stress along the radius direction which is given by  $\sigma_{rr} \sim \gamma a^2/r^2$  here  $\gamma$  is the surface tension at the

edge of the film,  $a$  is the radius of the droplet,  $h$  is the thickness of the film and  $E$  is the modulus of the film. Equation (8) can be rewritten as:

$$\lambda = C_\lambda a^{-1/2} r \left[ \frac{E}{12(1-\nu^2)\gamma} \right]^{1/4} h^{3/4} \quad (9)$$

$C_\lambda$  is a numerical constant. Since it is a radial wrinkle pattern,  $\lambda=2\pi r/N$ . So the relation between the number of wrinkles and the film properties could be established.

$$N = C_N \left[ \frac{12(1-\nu^2)\gamma}{E} \right]^{1/4} a^{1/2} h^{-3/4} \quad (10)$$

$C_N$  is a numerical constant.

Since the length of wrinkle is determined by the radial distance at which the value of stress resulting from the force applied at the center decays to the same value of the tension applied at the distant boundaries. This gives the following equation:

$$L \sim a \left( \frac{F}{a\gamma} \right)^{1/2} \quad (11)$$

Where  $F=2\pi a\gamma$  in their case. This gives  $L \propto a$ . Experimentally, a power-law scaling relation was found:  $L \propto ah^{1/2}$ . Using this experimental relationship along with dimensional analysis, the following semi-empirical relationship was found:

$$L = C_L \left( \frac{E}{\gamma} \right)^{1/2} ah^{1/2} \quad (12)$$

By combining equations (10) and (12), the thickness and film modulus could both be calculated simultaneously without known either one of them. Thus, this approach is a powerful way to characterize thin films as thin as a few hundred nanometers.

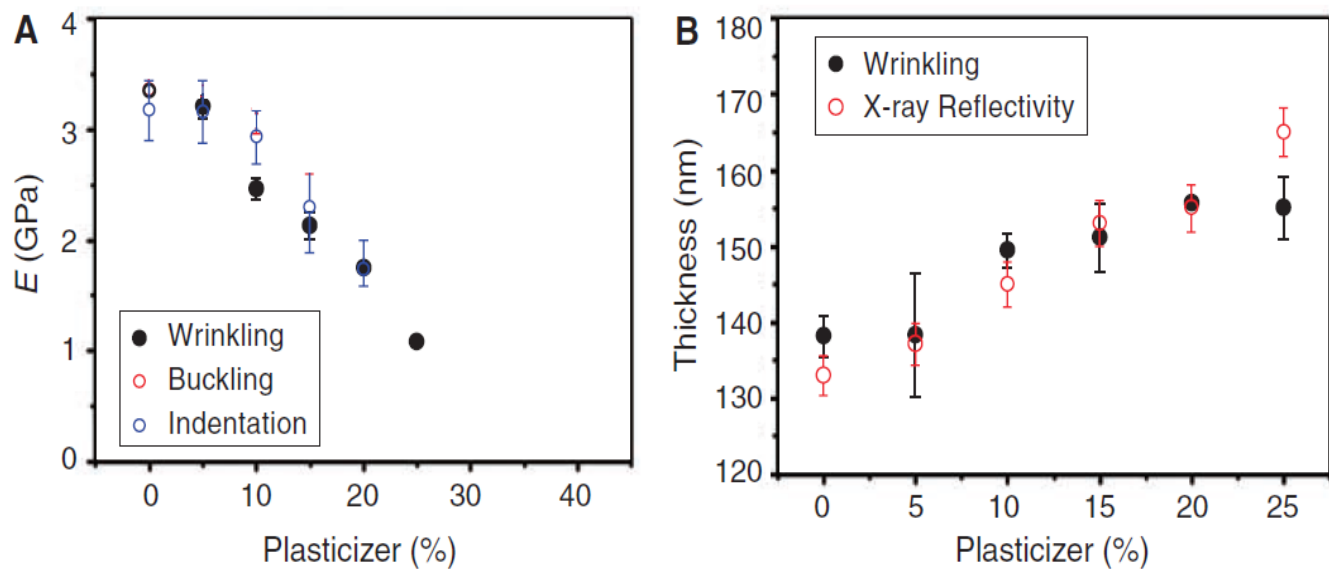


**Figure 4** Verification of Huang's Experiment(Huang et al, [25]).  
**Left:** Modulus obtained by wrinkling method as well as indentation methods. **Right:** Thickness obtained by wrinkling methods and X-ray reflectivity methods. Figure used with permission.

Indeed Huang et al verified that, the modulus obtained from the radial wrinkling method is close to the values from indentation methods, and the thickness of the film obtained from the radial wrinkling method also agrees well with the value from the X-ray reflectivity method.

### 2.2.3 Other buckling based measurements

As the complement of the study of wrinkling phenomena, the delamination which is also called “blistering” has been studied by Vella et al. By combining the relationship between wavelength and film properties as well as amplitude of blister with film properties; the interfacial toughness could be obtained.[4]

Additional film properties have been measured by Stafford et al[20]. With the increasing stretched strain applied on film, wrinkles first appear on the film surface and then cracks appear. The fracture strength of the film could be calculated by measuring the average width of fragments as well as the onset fracture strain.

In addition, quantitative evaluation of the interface adhesion by analyzing the geometry of indentation-induced delamination of thin films has been studied [16]

Also Chung et al observed surface wrinkling patterns in UV/ozone (UVO)-treated polymer films exposed to solvent vapor [28]. They observed the wrinkle patterns such as “spokes” and “targets”, and the wrinkle growth rate were found to strongly depend on the rate of solvent diffusion into the film. A connection between diffusion kinetics and pattern morphology was found, thus allowing diffusivity to be measured by monitoring wrinkle formation.

Stafford et al evaluated residual stress in nanoscale polymer films by monitoring the onset of strain-induced wrinkling instabilities [29]. In their work, the strain measured in the onset wrinkling point is defined as critical strain which is also one important parameter that studied in our project.

#### **2.2.4 Research on films coupled with viscous substrate**

The experiments mentioned above all require that mechanical equilibrium be reached between elastic forces in the film, and other forces such as elastic forces in a soft solid substrate or surface tension forces, or gravity. We seek to apply these methods to molten polymers which are highly viscous. A typical example is the molecular film generated by an interfacial coupling reaction between immiscible polymers. In such cases, mechanical equilibrium is more difficult to reach, because the physical process is no longer controlled by substrate viscosity rather than the elastic force or gravity, therefore the methods reviewed in the previous section cannot be applied directly. Instead, relatively slow time-evolution of wrinkles is expected; besides, considering the tight bond between the viscous substrate and the thin film, a non-slip boundary condition is usually applicable. The goal of this research is to relate wrinkling characteristics in such viscous systems to the mechanical properties of the films.

Wrinkling on highly viscous fluid substrate has been noted previously. For example, Hobart et al [5] transferred a pre-compressed 5 nanometer SiGe film on to a Si substrate covered with the borophorosilicate glass (BPSG), and heated this bilayer system above the glass transition temperature. Since the film tries to increase its area due to the compressive pre strain, buckling generated wrinkles as shown in Figure 5.

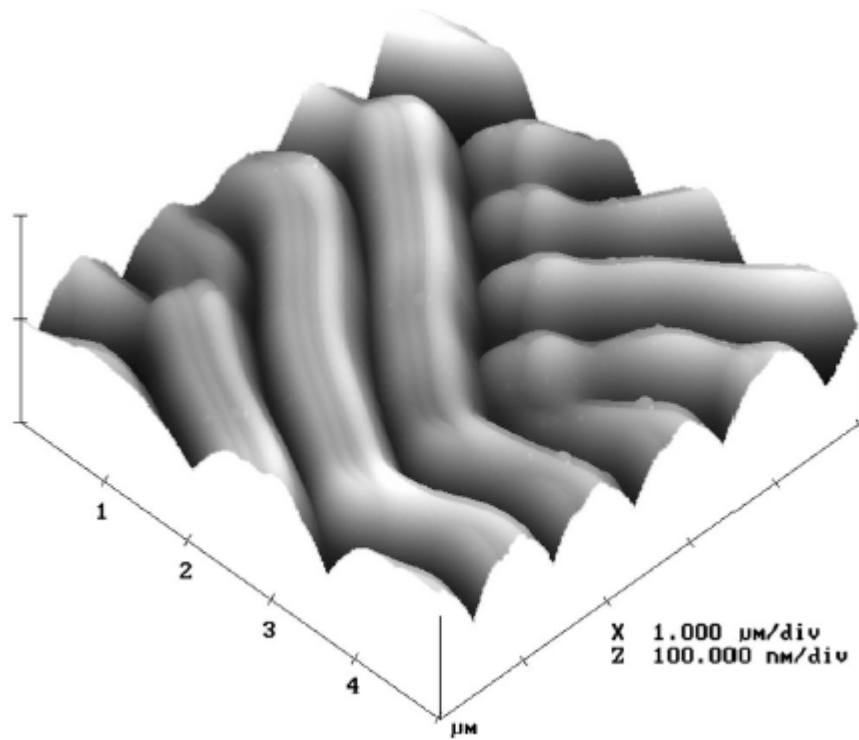


**Figure 5** AFM image of buckled SiGe film on BPSG after 800°C, 90 min annealing.

Theoretical analyses have been carried out for wrinkle model with controlled strain [30-32] Sridhar et al applied lubrication theory to the viscous substrate as well as nonlinear thin plate theory to describe the thin film. Recently, Huang et al[33] carried out the theory analysis based on this model. Via applying the lubrication theory on the fluid and nonlinear theory on the film a relation between the displacements and film properties has been developed. Then they carried out a linear perturbation analysis on the displacements of the surface of viscous layer as well as the displacement perpendicular to the surface assuming plane strain conditions. The critical wave number and wrinkle growth rate of this unstable model were found.



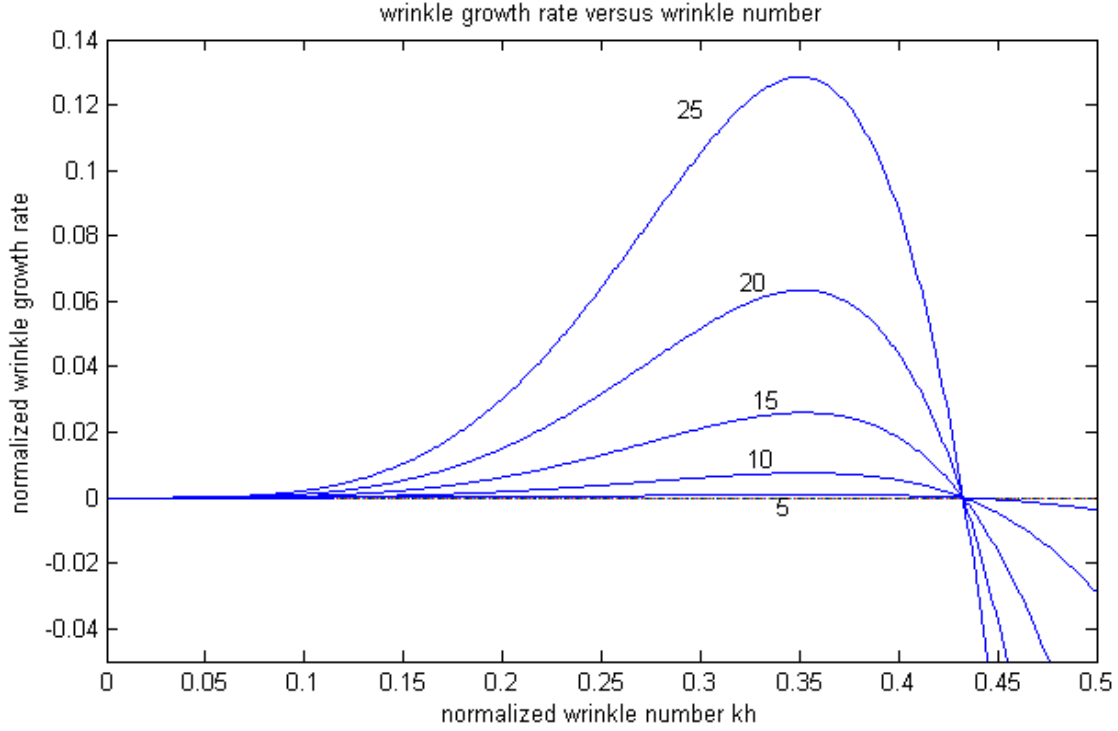


**Figure 6** Normalized growth rate with respect to the normalized wave number. The numbers next to each curve indicate the thickness ratio  $H/h$  between the viscous layer and the film. The pre strain is -0.012 and Possion ratio is 0.3.

In Figure 6 the normalized wrinkle number is  $kh = \frac{2\pi}{\lambda}h$ , where  $h$  is the film thickness [m]. Similarly, normalized growth rate is the growing speed of the wrinkle [ $s^{-1}$ ] multiplying substrate viscosity  $\eta$  [ $Pa \cdot s$ ] and divided by film modulus  $E$  [ $Pa$ ].

From Figure 6, for one single curve we could see for  $kh \rightarrow \infty$ , the wrinkles have short wavelength. Since the bending energy is too high to trade off with the in-plane deformation energy, the wrinkle decays. In contrast, for  $kh \rightarrow 0$ , the wavelength is large and the viscous substrate needs a long time to flow and accommodate the film bending, and hence wrinkles grow slowly. The value of wave number beyond which wrinkles start to decay is marked as the critical wave number in the figure. From this analysis, they concluded that the wrinkle wavelength appearing on the film is the one with the maximum growth rate. Besides, Figure 6 shows when

the thickness ratio reduces, the value of maximum growth rate reduces and the wave number corresponding to the maximum growth rate increases. Meanwhile, the critical wave number does not change at all since it depends on the film properties and pre strain only.

However, for the case discussed above the strain is from the pre stressed film and cannot be controlled well. Thus, it cannot be applied externally as desired. In our project, we will develop a method to apply controlled compressive strain on the bilayer at a controlled rate.

### **3.0 MATERIALS AND METHODS**

As mentioned in the previous chapters, the general idea of this thesis is to develop a method to measure the mechanical properties of the interface between two immiscible fluids. The real life cases of interest concern interfacial films that are formed by a chemical reaction between two immiscible polymer species. The focus is on using buckling methods, more specifically, the major task of this project is to capture and analyze wrinkle pattern of the thin film resulting from the process of compressing a high viscous substrate supporting it. The effects of experimental parameters (the thickness of the viscous substrate and the compression rate) on the wrinkle pattern have been tested out in this project.

In our project, the majority effort has been made on developing the measurement method itself. So instead of working on the reactively generated film, a much thicker film (few micron scale) has been use as experiment sample. There are two advantages: 1) the thicker film is much easy to handle, and the experiment conditions are more reproducible as compared to the reactively generated film whose generation has been mentioned in Appendix. 2)the properties of the film , e.g. the thickness and modulus, are well known, they can be used to validate the accuracy of the new buckling method. Moreover the experiments are done at air/polymer interfaces rather than polymer/polymer interface.

### 3.1 EXPERIMENT DESIGN

A polymeric film which attaches to a high viscous liquid can form wrinkle patterns while the viscous liquid provided it with a compressive strain. Figure 7 shows the conceptual figure of the experiment.

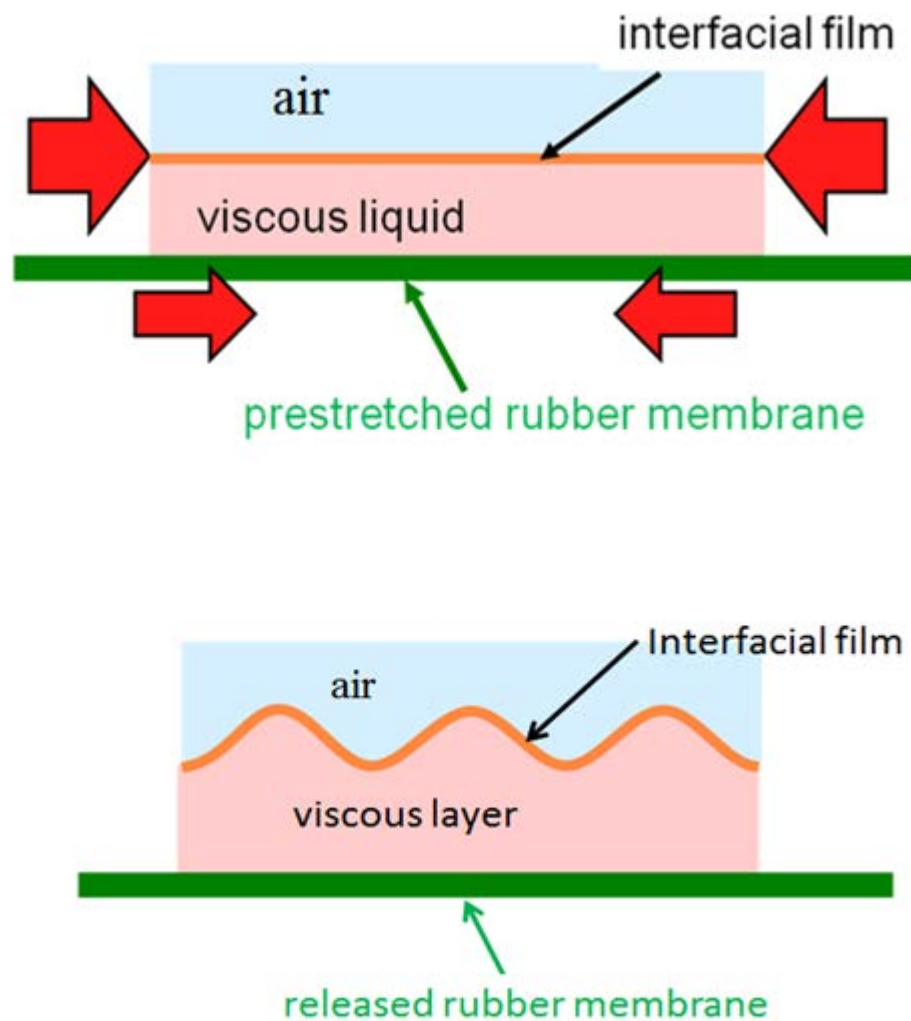


Figure 7 Schematic of the flat and the wrinkled states of a polymeric film on a highly viscous layer. The layer is supported by a pre-stretched rubber layer membrane.

The experiment system in this study is shown in Figure 8. It consists of three parts: the Instron, the rail-carriage assembly, and the rubbery tray.

The general experiment steps are: pre-stretch the rubber tray using the displacement provided by the Instron tensile testing machine, hold this state for a sufficiently long time to ensure that the highly viscous substrate is dispersed uniformly in the tray, and the film remains flat and level on the substrate. Then release the rubbery tray at a controlled speed up to a controlled displacement. The resulting wrinkling of the film is recorded by video camera.

The Instron machine used to provide controlled displacement for this experiment shown in Figure 9. The left part of Figure 9 is a photo of model 4202 Instron, the right part of Figure 9 is a sketch of the modifications made : a metal pulley is fixed to the base so that the vertical travel of the crosshead of the Instron machine is converted into a horizontal displacement.

The stand that is designed for supporting the rubber tray is shown in Figure 10. The two ends of the tray are clamped between the upper and lower plates, allowing the tray to be stretched or upstretched in a controlled fashion. Figure 11 is a schematic of the tray made of P-10 silicone rubber. Each edge of the tray is clamped between the upper and bottom plate of the stand.

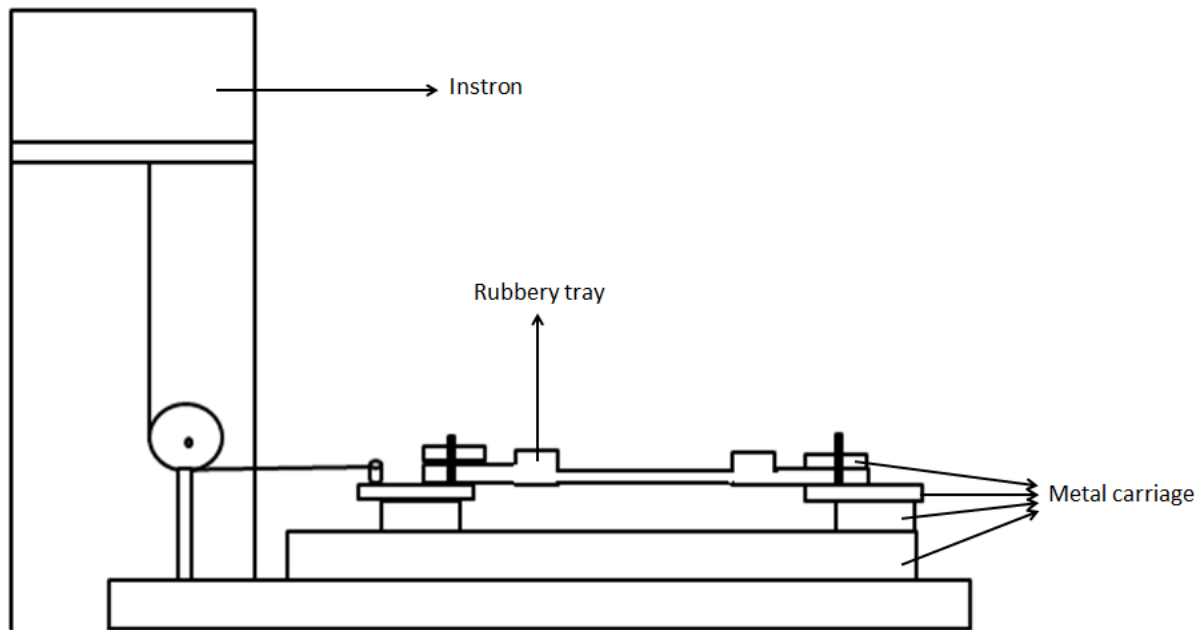


**Figure 8** The general experiment system design.  
The system consists of an Instron machine for controlling displacement, a rubbery tray, and a metal carriage.

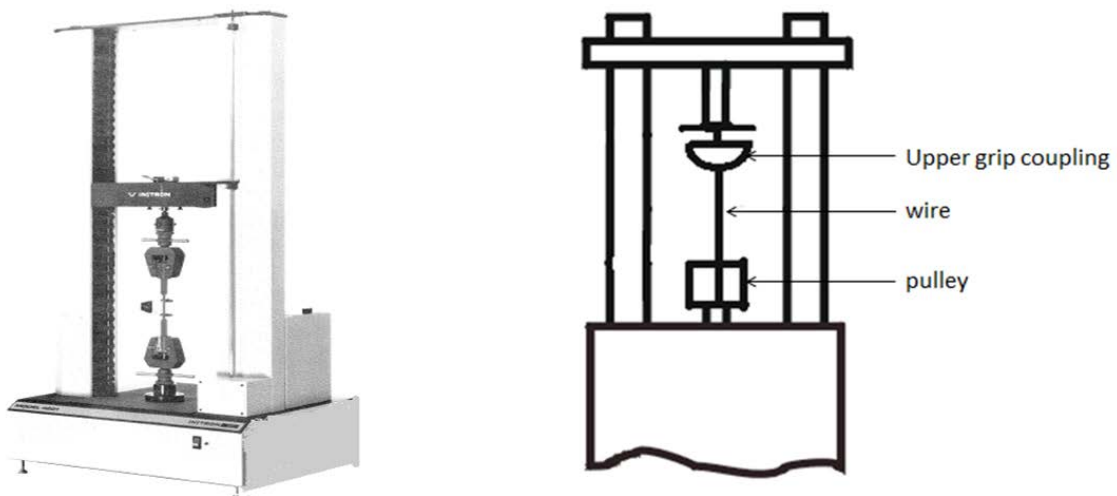


**Figure 9** A photograph and a schematic sketch of the Instron tensile testing machine.

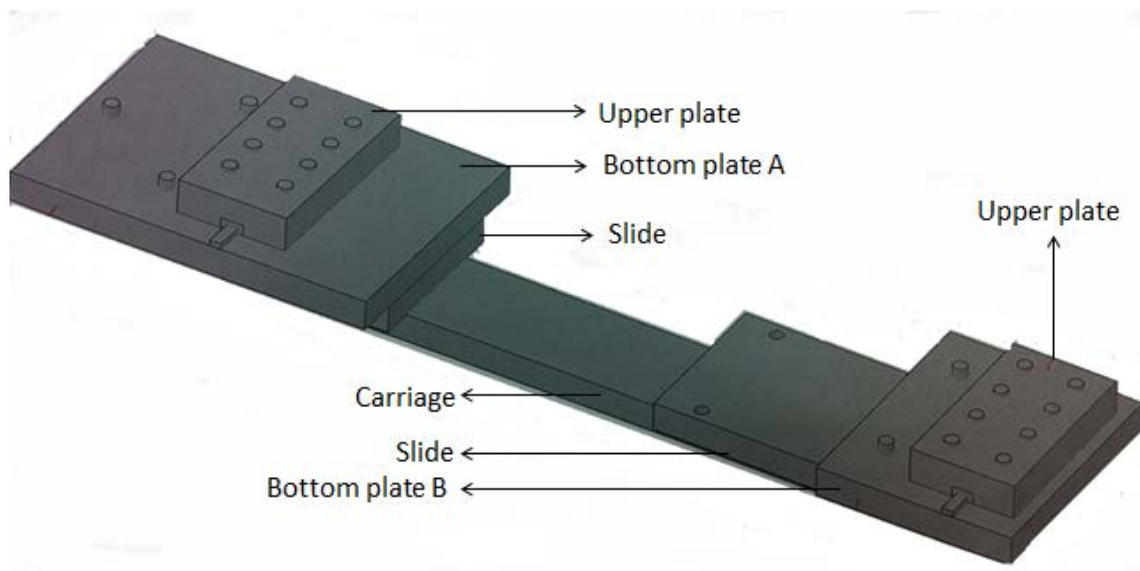


**Figure 10 The rail-carriage assembly.**

It consists of the upper and bottom plate that is used to clamp the edge of the rubbery tray as well as the slide and carriage which allow the plates move in one direction.

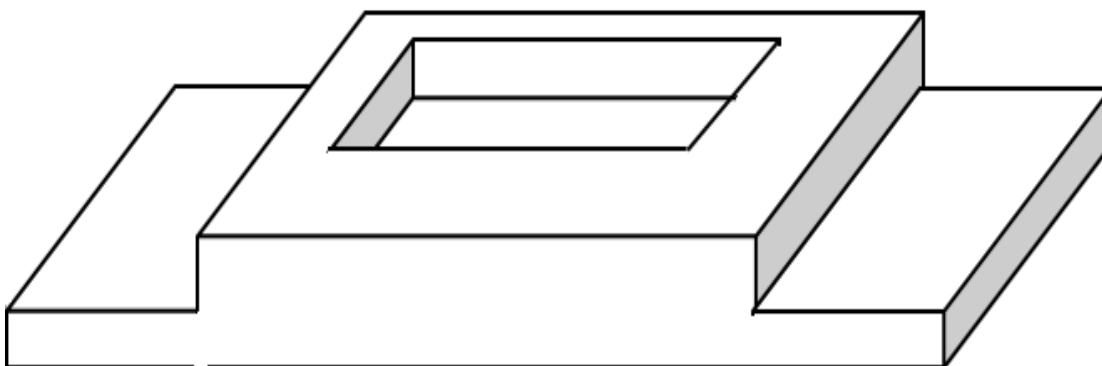


**Figure 11 The silicone rubber tray.**

In the experiment, the rubber tray is filled with a highly viscous liquid polymer. A polymeric thin film is placed on the surface of the liquid polymer.

### 3.2 MANUFACTURE OF RUBBER TRAY

P-10 special effect silicone is used to make the rubber tray in this project. It is a two component condensation cure silicone rubber. The two components (the base and the activator) are fully mixed with a mass ratio of 10:1 (base: activator=10:1). The mixed silicone is degassed in vacuum and poured into an acrylic mold which is a “negative” of the desired tray. The mold is allowed to sit on a level bench for 24 hours. The tray made of this silicone possesses extremely high elongation, and the very low durometer of the silicone allows maximum flexibility. Therefore it can be easily and uniformly stretched, thus allowing the viscous substrate to be stretched and compressed. Moreover, after mounting the tray on the carriage, another thin layer of P-10 was poured in to the tray. Due to the self-leveling properties of P-10, the surface of the tray will be approximately flat..

In order to ensure the bottom surface of the tray was completely level (i.e. perpendicular to gravity) after it is mounted on the carriage, another layer of mixed p-10 silicone was poured above the tray surface where it self-leveled under gravity before curing. After it is cured, the bottom surface of the tray is complete flat and level.

**Table 1 Typical properties of the P-10 silicone.**

component	color	Viscosity(cps)	Working time(hrs)	Cure time(hrs)	Specific gravity,cured	Elongation (%)	Shelf life
base	translucent	15.000	1-2	16-18	1.08	450±50	6month
activator	pink	300-400					



### 3.3 DATA MANAGEMENT AND IMAGE CAPTURE

The model 4202 Instron is controlled by a control board, and connected to a computer. The releasing rate and displacement of the Instron are controlled and recorded by software (Lab-view). The process of appearance and relaxation of the wrinkle pattern is recorded by a Panasonic SDR-T70 camcorder. Figure 12 shows the experiment setup and light path during the recording time.

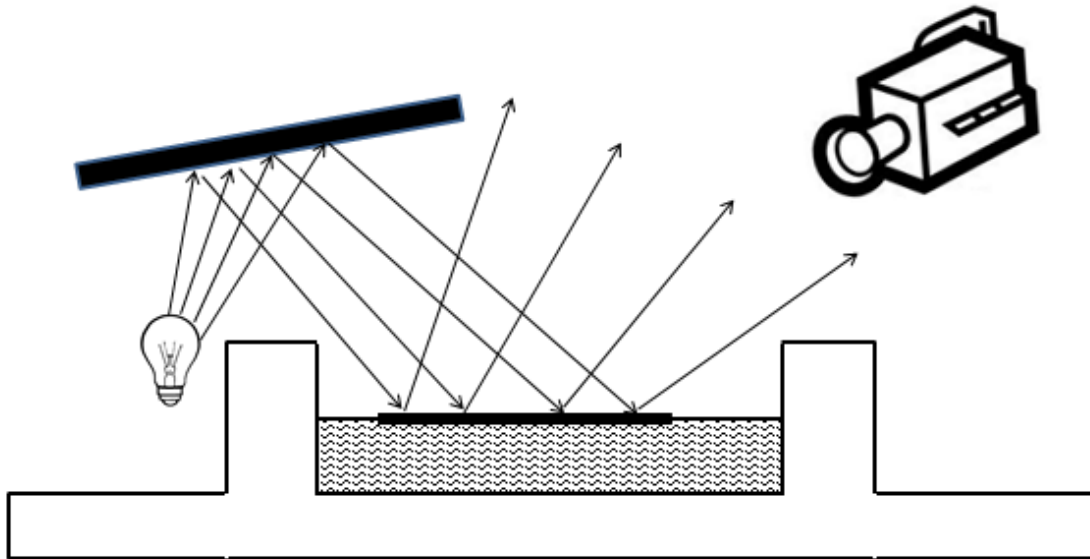


**Figure 12 Setup of the recording devices.**

The diffuse reflection of the light bulb from a rough surface illuminates the thin film placed on the viscous substrate. The camcorder captures the reflected light from the film.

### 3.4 MATERIALS

Polyisoprene polymer LIR-50 is used as the viscous substrate. Its properties are summarized in Table 2. The samples used in the experiment are 5 $\mu$ m thick clear polyester Mylar films purchased from homefly.com. This material is strong, inert to water, and unaffected by oil, grease, and most aromatics. More importantly it is readily available in large quantities, thus saving the considerable trouble in preparing our own thin films for this research.

**Table 2 Typical properties of LIR-50.**

Name	Type	Molecular weight	Melt viscosity (Pa·s at 25°C)	Specific Gravity (g/cc)	Glass transition temp. (°C)	Structure
LIR-50	homopolymer	54000	1170	0.91	-63	$\left[ \text{CH}_2 - \overset{\text{CH}_3}{\underset{ }{\text{C}}} = \text{CH} - \text{CH}_2 \right]_n$

## 4.0 RESULTS AND DISCUSSION

### 4.1 EXPERIMENTAL PROCEDURE

The rubber tray was pre-stretched by Instron 4202. The initial stretching displacement was 15mm and the length of the tray was 165mm. This corresponds to a 9.1% stretching. The desired amount of LIR-50 was poured into the tray and allowed to stay quiescent for at least 10 hours to ensure that the surface of LIR-50 was flat. The LIR-50 layer thickness was obtained as described in the following paragraph. The 5 $\mu$ m thick clear polyester Mylar film was placed on the surface of LIR-50 layer. Figure 13 shows the method of placing the film on the substrate surface without getting air bubble in between these two layers.

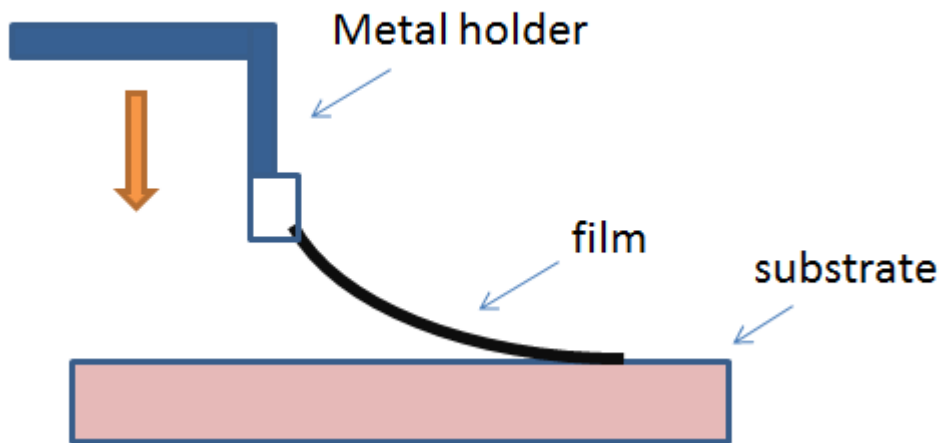


Figure 13 Placement of a film on the liquid substrate.

One edge of the film was attached to a metal holder connected to the crosshead of the Instron. The other end was allowed to contact the liquid surface and then laid down slowly from the other edge by controlling the Instron speed at about 5mm/min.

After the film was deposited on the surface, the pre stretched tray was released at a fixed velocity. Wrinkles formed once the pre stretching had been released to a certain extent. This entire process was recorded with a camcorder. The video was transferred from camcorder to a computer, individual frames were extracted, and parameters such as strain, strain rate, and wrinkle wavelength were estimated.

#### **4.1.1 Method of measuring substrate thickness**

We assume LIR-50 layer has a thickness  $H$ , and the surface area of the tray is  $S=W*L$  where  $W$  is the width of the tray and  $L$  is the length, the mass of LIR-50 needed is  $m=\rho*W*L*H$ , where  $\rho=0.91\text{g/cm}^3$ . Thus in most experiments, the desired weight  $m$  was poured into the tray. However due to the edge effects, the thickness obtained was expected to deviate from the calculated value. Accordingly, a micrometer was used to measure exact thickness of the LIR-50 layer as showing Figure 14.



**Figure 14 Measurements with the micrometer.**

While the tray was initially empty, the micrometer drive was adjusted until the lens contacted the bottom surface of tray, and this micrometer position was recorded as a zero. Then the LIR-50 fluid was poured in, and allowed to settle until the surface became completely flat. The micrometer was readjusted, so that the lens just touched the surface of LIR-50 to obtain the thickness of the liquid layer.

The contact of the lens with either the rubber surface or the liquid surface could be observed very readily. A circle formed in the center of lens as soon as contact occurred as shown in Figure 15.



**Figure 15 The contact between the lens and the surface.**

The left panel is the top view of the lens contacts with the rubber tray, the right panel is the top view of the lens contacts with the surface of liquid. Arrows have been added to indicate the contact circle.

In order to test the accuracy of this method, we placed a 1.600mm thin rubber sheet in the tray, and measured its thickness with the above method three times. The values obtained were 1.611mm 1.687 mm 1.653mm, indicating a variability of less than 100  $\mu\text{m}$ .

#### 4.1.2 Method of obtaining wrinkle wavelength from image

A ruler was placed in the middle of tray where wrinkle was being observed, and a certain distance X was taken as the reference.

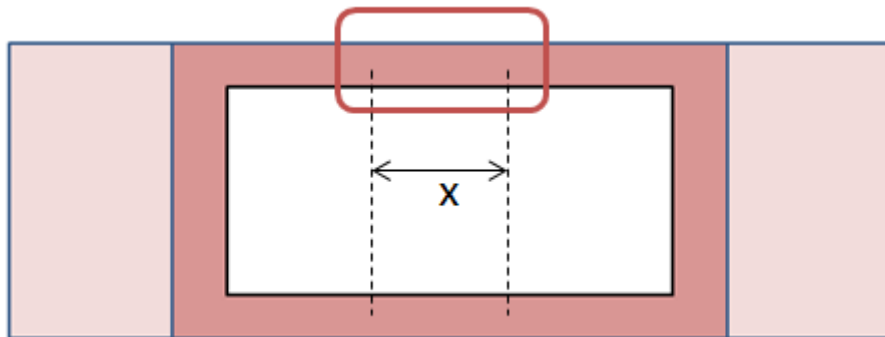


**Figure 16 Schematic of the video recording region.**  
The red rectangular is the region recorded by camcorder, and X is the distance taken as the reference.

The number of wrinkles N within this distance X was counted and wavelength of wrinkle calculated as

$$\lambda = \frac{X}{N} \quad (13)$$

The number of wrinkles counted from our experiments ranges from 4 to 18. Since some uncertainty exists in the counting process which depends on the video quality, lambda can be regarded as accurate to within

$$\frac{X}{N-1} > \lambda > \frac{X}{N+1} \quad (14)$$

#### 4.1.3 Strain rate calculation

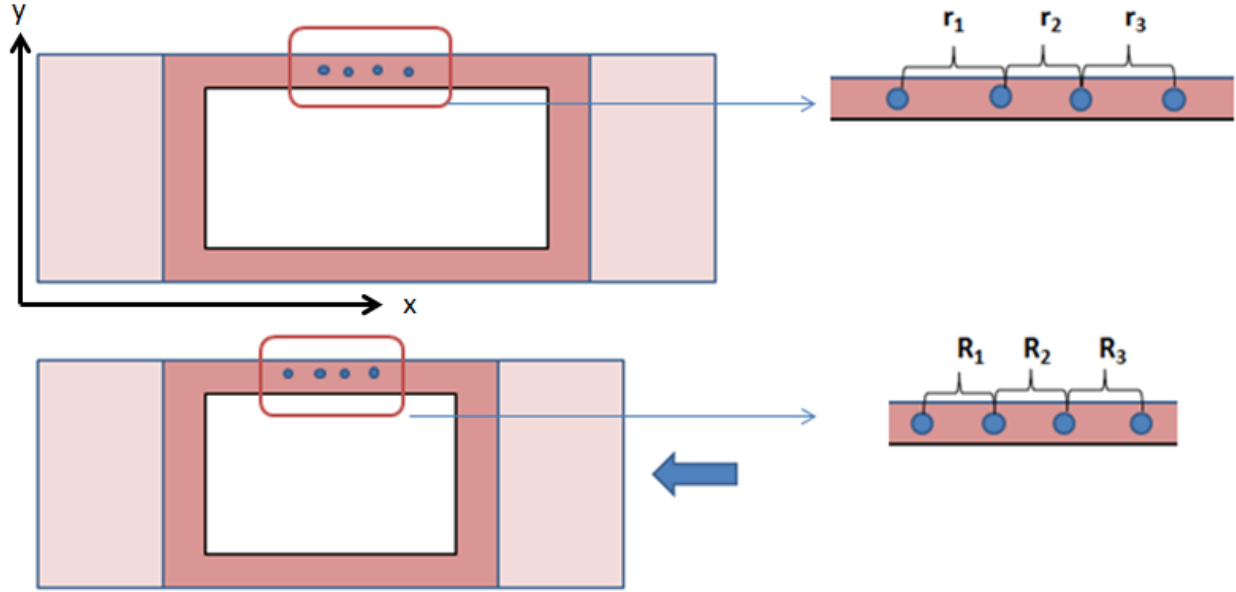


**Figure 17 Schematic of the markers movements.**

The top left panel shows the tray under initial stretch condition and the blue spots serve as markers on the wall of tray. The bottom left panel shows the tray after certain releasing time  $t$ , the right part is the detailed view of the center of tray, where the camcorder was placed and the strain releasing process was recorded.

The tray is pre-stretched in  $x$  direction. Ink spots were placed as markers on the edge of the tray. During the releasing of the pre strain, the displacement of the markers was monitored and then used to calculate the strain rate. The entire procedure will be illustrated in the next section.

The strain could be calculated as:

$$\varepsilon = \frac{\sum_{i=1}^n (r_i - R_i)}{\sum_{i=1}^n r_i} \quad (15)$$



Where  $R_i$  and  $r_i$  have been indicated in Figure 17. This part of calculation was done by a Matlab program written by Dr. Sourav Chatterjee.

The strain rate could be obtained as the slope of the strain versus time data. Moreover, once the strain rate was calculated, the critical strain could be calculated by multiplying it with the time for the appearance of wrinkle.

## 4.2 VALIDATION EXPERIMENTS

First, we measured strains of different positions on the tray wall along the releasing direction according to equation (15).



**Figure 18** Video frames illustrating the displacement of the markers.

By tracking the movement of the markers with the mentioned Matlab program, we obtained Figure 19.

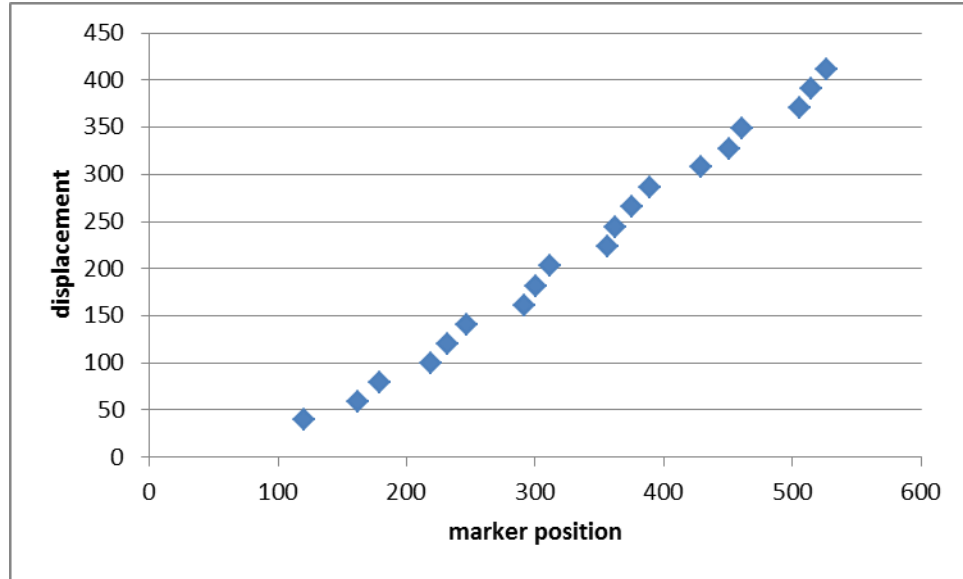


**Figure 19 Marker displacements versus positions after 0.17s**

The markers' displacements have a linear relation with their position according to Figure 19, so their slope is a constant. In other words, strain is approximately uniformly distributed along the releasing direction in the tray part we are observing.

Then we validated the variation of strain during the releasing process. Three figures with data recorded under different instron releasing velocities for the whole releasing process have been presented below.

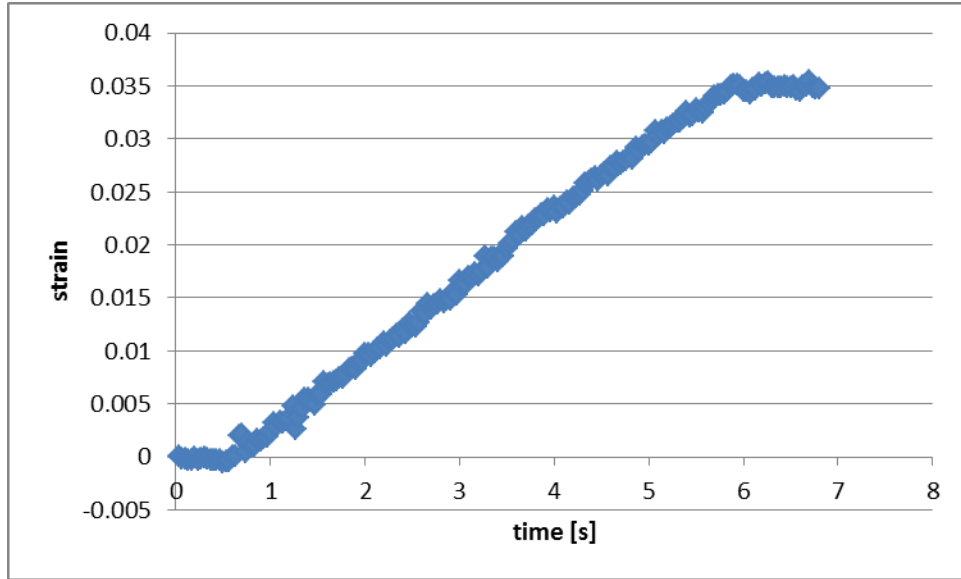


**Figure 20** Strain versus time during the whole releasing process. Instron velocity: 100 mm/min.

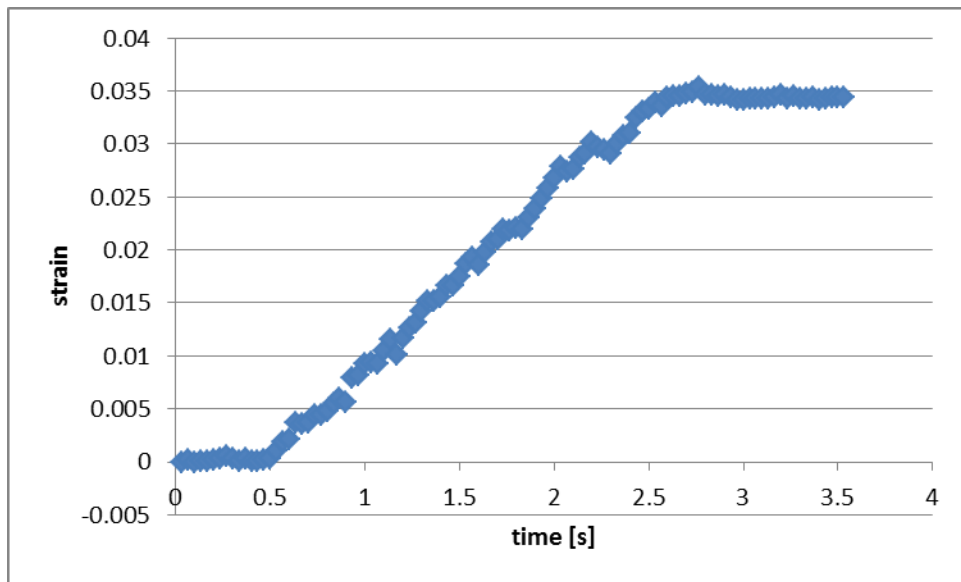


**Figure 21** Strain versus time during the whole releasing process. Instron velocity: 300 mm/min.

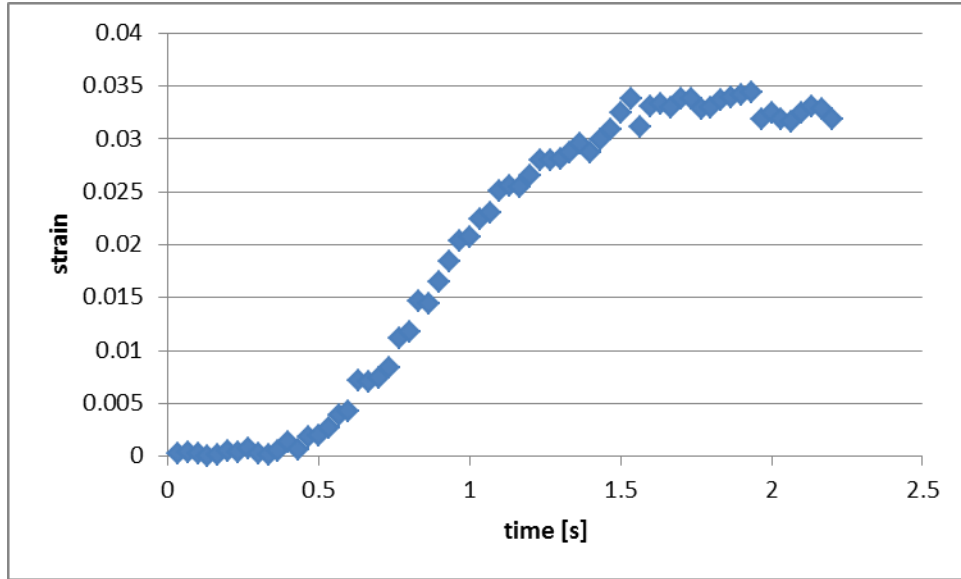


**Figure 22 Strain versus time during the whole releasing process. Instron velocity: 500 mm/min.**

Figure 20-22 show the change of strain experienced by the tray during the releasing process. Initially, the tray is pre-stretched and hence there is no change in the deformation of tray, thus the strain is zero and does not change with time. As the tray is released, strain increases until the release is stopped at which point the strain stops changing again.

From the figures, during the release process, the strain increases approximately linearly with time which indicates that the strain rate is roughly constant during the releasing process. However at the very beginning of the releasing process, there is a gradual increase in rate. This will create uncertainty of the critical strain since it obtained at that time period.

Moreover, the strain rate changes with different releasing velocity provided by the Instron. In order to validated the relation between these two parameters. We plot the instron velocity versus the calculated strain rate in Figure 23.

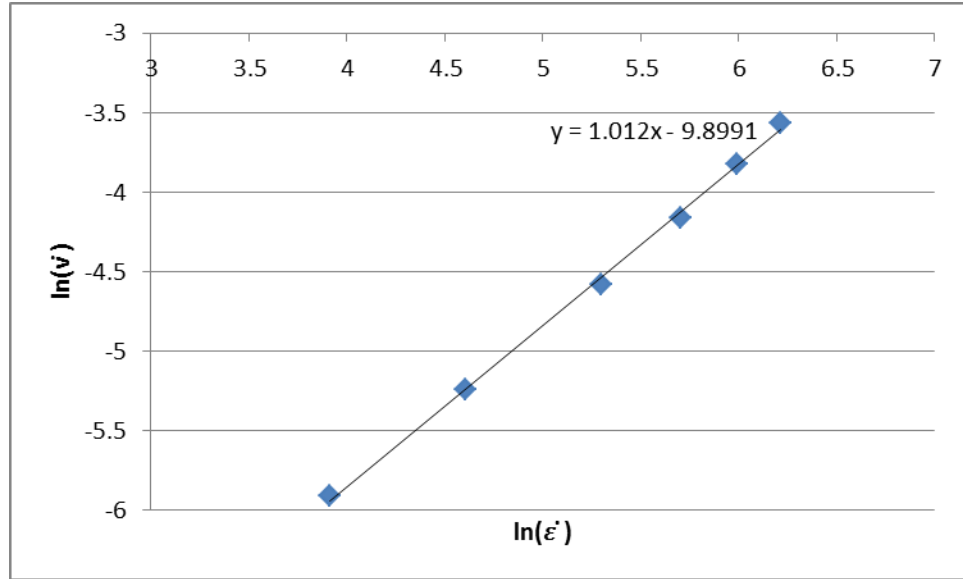


**Figure 23 Instron velocity versus calculated strain rate.**

The slope of this plot on the log-log scale is almost exactly 1 indicating that the strain rate is nearly proportional to the release velocity.

However, the value of critical strain obtained in our project which mention in the next section are fairly small, therefore, the highest strain rate obtained by this method prior to wrinkling may somewhat lower than the value obtained from fitting the linear part of the curve.

## 4.3 RESULTS

### 4.3.1 Wavelength versus strain rate

In order to find the relation between the wavelength and strain rate, experiments have been carried out under different strain rates while other experiment conditions remain the same. The releasing velocities ranged from 50mm/min to 500mm/min corresponding to strain rates ranging

from  $0.0030\text{s}^{-1}$  to  $0.030\text{ s}^{-1}$ . With the methods mentioned in section 4.1 the values of wavelength and strain rate could be obtained.

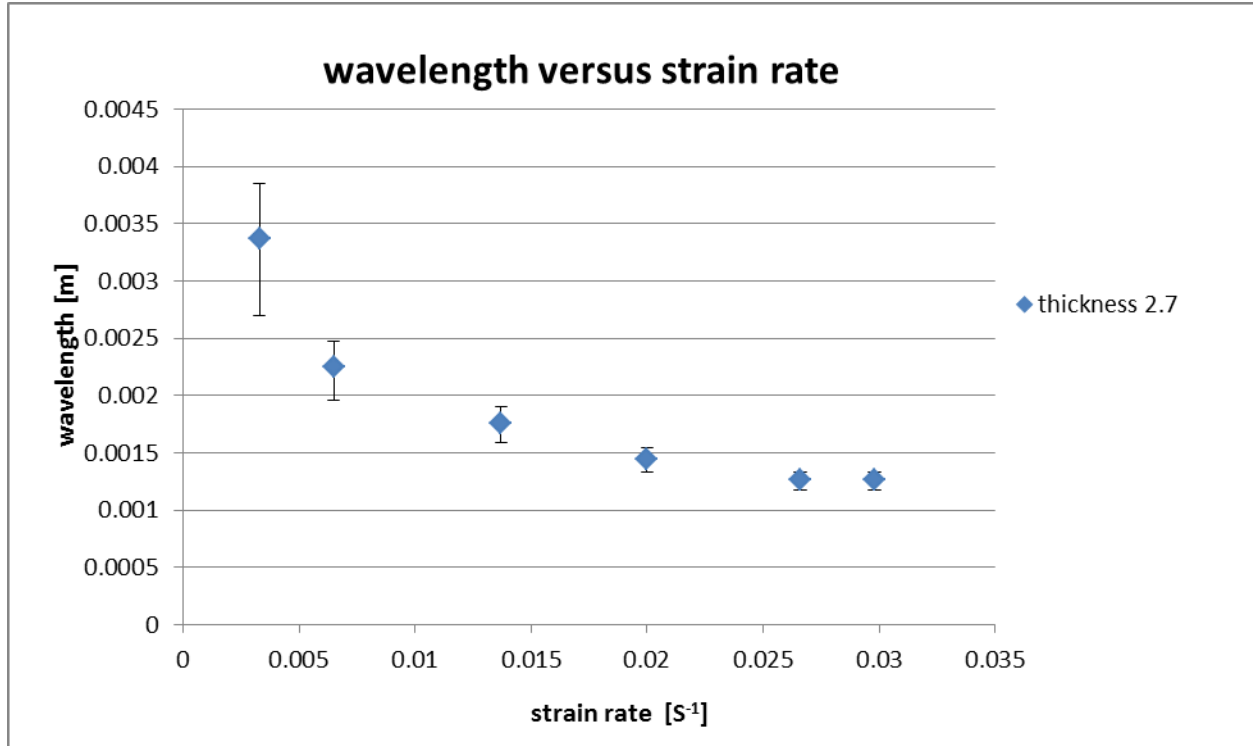


**Figure 24 Wavelength verses strain rate. Thickness: 2.7mm**

The thickness of viscous layer is 2.7 mm. the error bar was calculated by adding and deducting one wrinkle during counting the number of wrinkles.

From Figure 24, it is clear that with the increase of strain rate, the wavelength of the wrinkle decreases.

#### 4.3.2 Wavelength versus viscous layer thickness

Experiments upon different substrate thickness and different strain rate have been carried out. The range of liquid substrate thickness is from 5 mm to about 1 mm.

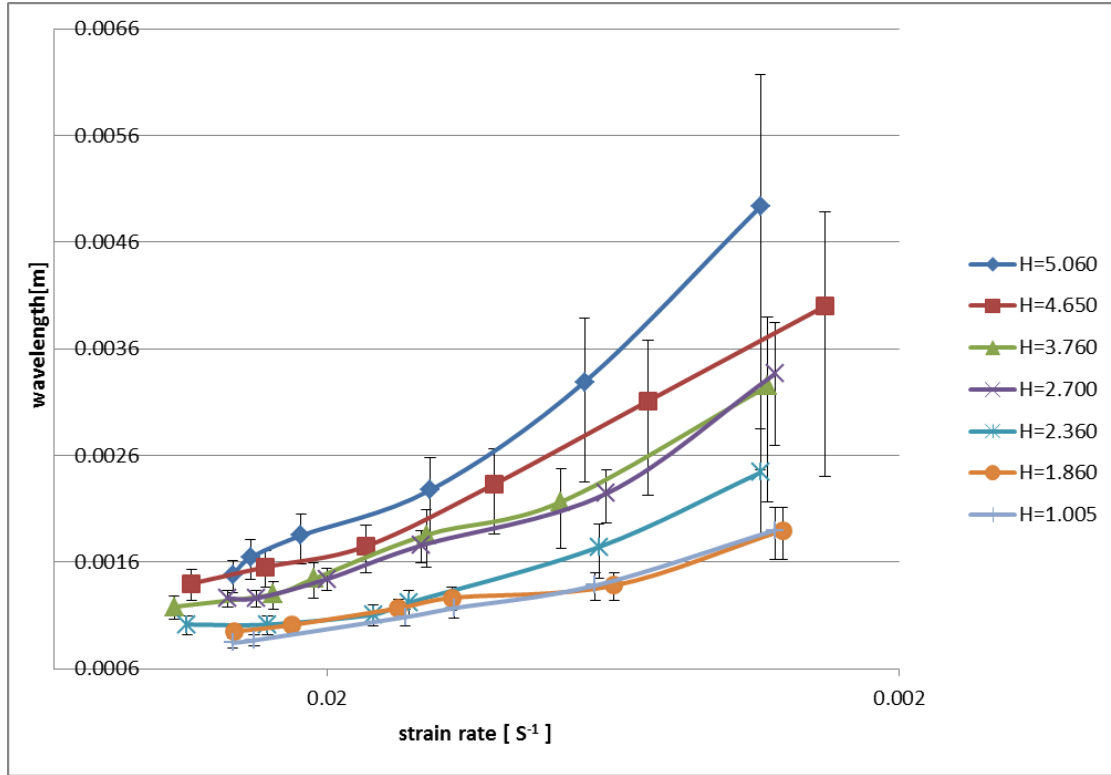


Figure 25 Wavelength verses strain rate. Thickness[mm] varies.

From figure25, there is still an obvious trend that the wavelength decreasing with increasing strain rate for any thickness ratio which agrees with the observation we had in the section 4.3.1. Furthermore, the wavelength (at any given strain rate) reduces with decreasing liquid substrate thickness. However, it appears that at small substrate thicknesses or at high compression rates, the dependence on substrate thickness is weak.

### 4.3.3 Critical strain versus strain rate

Also we are interested in the strain for the onset of wrinkle which we defined as critical strain in this thesis.

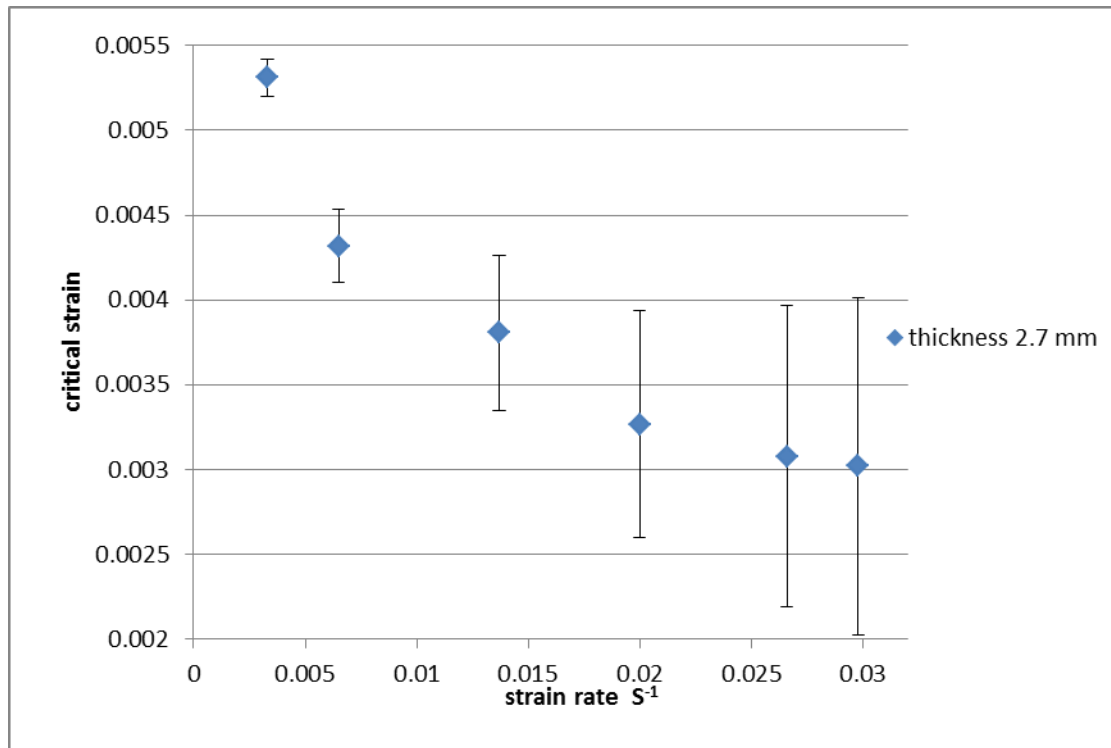


Figure 26 Critical strain verses strain rate. Thickness: 2.7mm.

The thickness of viscous layer is 2.7 mm. the error bar was calculated by strain rate multiplied the time for one single frame.

We see that with the increase of the strain rate, the strain need for onset wrinkle decreases. Moreover, in all cases, the critical strains are very small, far less than 1%. i.e. even a small amount of compression is sufficient to induce buckling in this situation.



#### 4.3.4 Critical strain versus substrate thickness

Experiments upon different substrate thickness and different strain rate have been carried out.

The thickness we choose are 5.06 mm, 4.65mm, 3.76 mm, 2.7 mm, 2.38mm, 1.86mm, 1.005mm.

The critical strains were obtained under these experiment conditions.

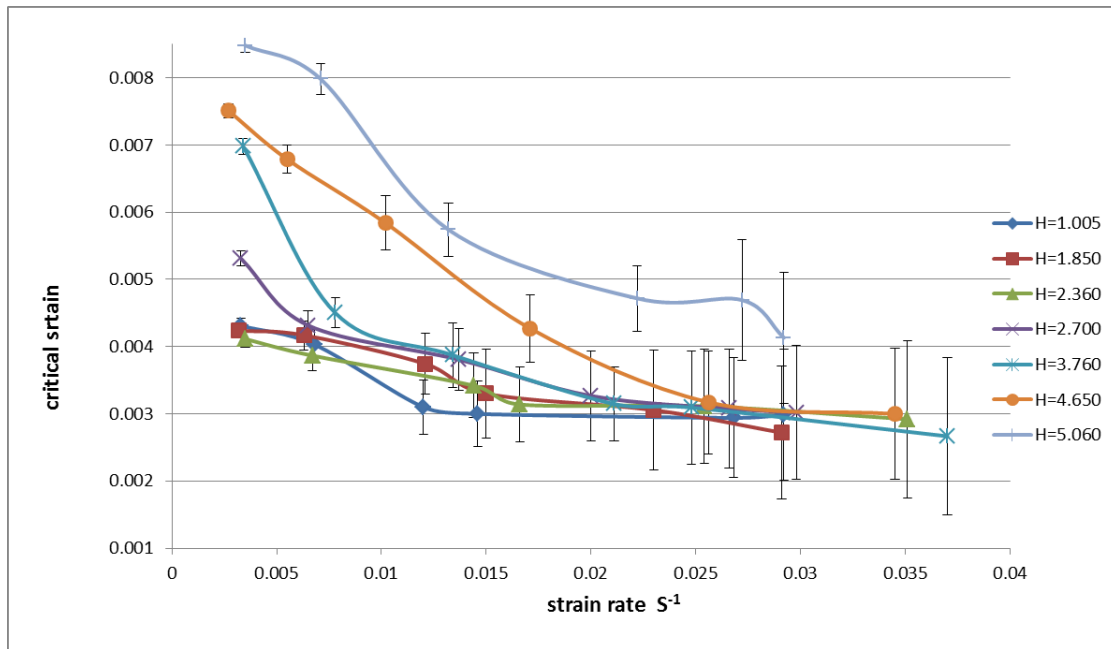


Figure 27 Critical strain verses strain rate. Thickness [mm] varies.

The value of critical strain drops with the decreasing of the substrate thickness.

## 4.4 DISCUSSION

### 4.4.1 Data normalization

The physical quantities we had in our experiment are presented in Table3.

**Table 3 Parameters in the experiment.**

parameters	strain rate	Substrate viscosity	Film modulus	Wavenumber	Film length	Film thickness	Substrate thickness
symbol	$\dot{\epsilon}$	$\eta$	$E$	$K$	$L$	$h$	$H$
Unit	$s^{-1}$	Pa*s	Pa	$m^{-1}$	m	m	m

In Huang and Suo's work[33]they normalized the wavenumber by multiplied it with the film thickness  $h$ , in order to get a consistent with their work, we also calculated the non-dimensional wavenumber  $kh$  according to our experiment result. Besides, dimensional analysis suggests that the only relevant parameters left are  $\frac{H}{h}$ ,  $\frac{L}{H}$  and  $\frac{\dot{\epsilon}\eta}{E}$ .

Figure 28 and 29 are the experiment data and normalized data respectively.

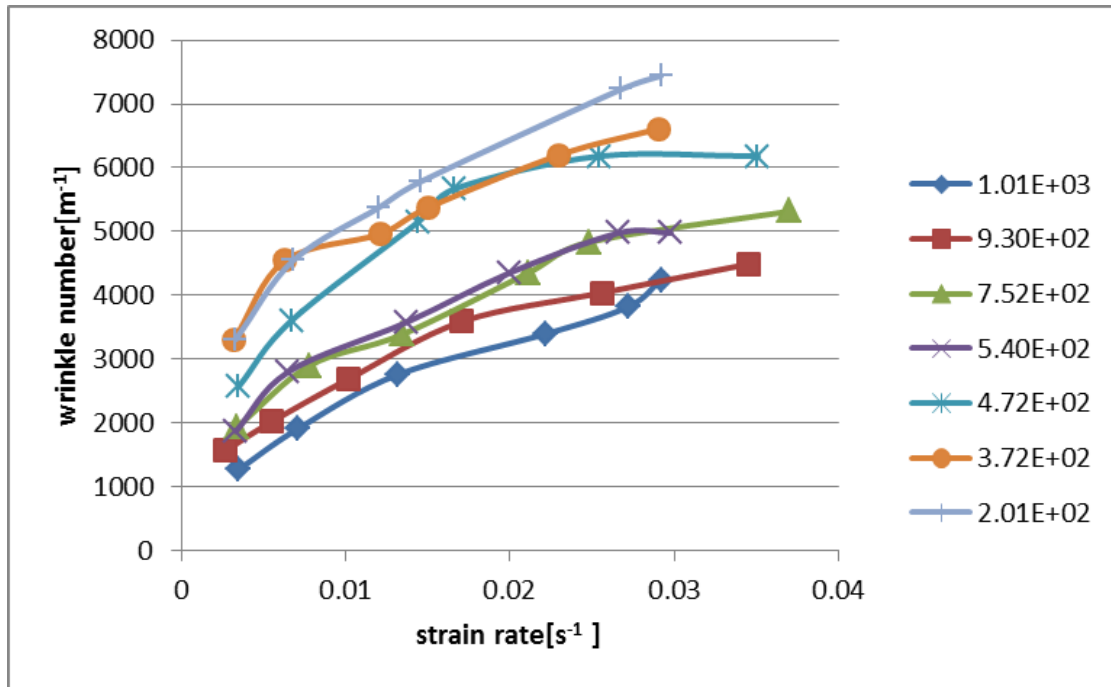


**Figure 28 Wrinkle number versus strain rate. Thickness ratio varies.**  
The thickness ratio is  $H/h$  where  $H$  is the substrate thickness and  $h$  is the film thickness that has been fixed to be  $5\mu\text{m}$  in our case

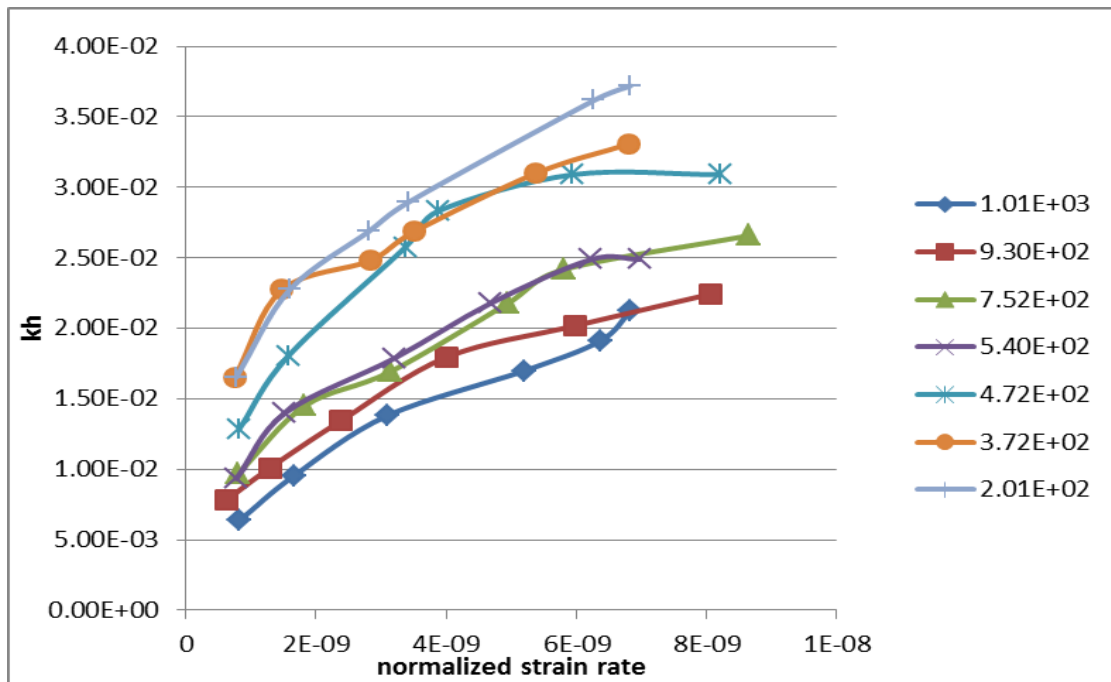


**Figure 29 Normalized wrinkle number versus normalized strain rate. Thickness ratio varies.**  
In addition, experiments with two different viscous substrates have been carried out

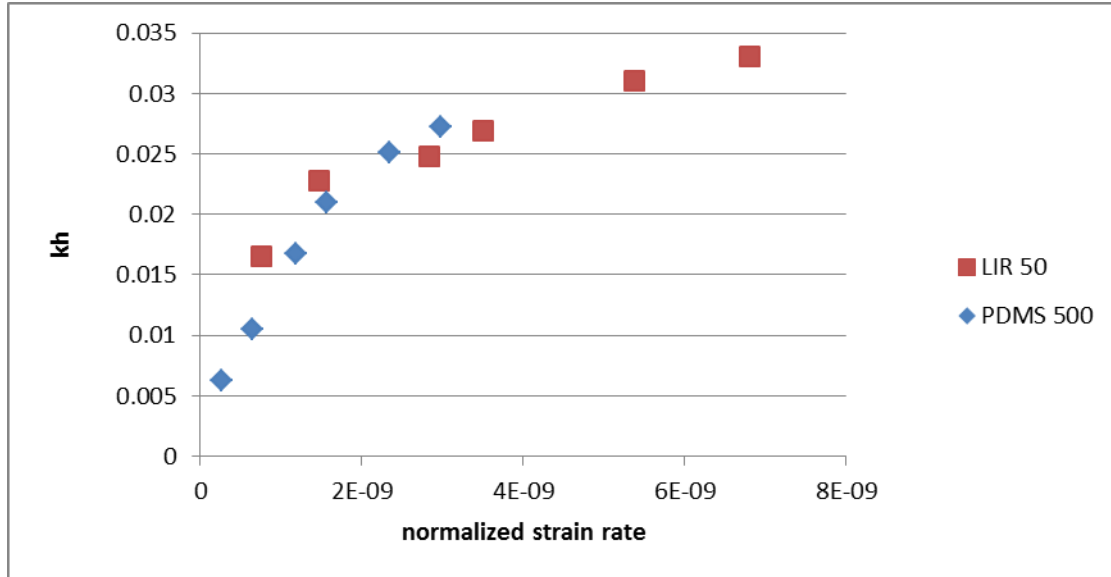


**Figure 30 Normalized wrinkle number versus normalized strain rate for two different viscous substrates**

Under same value of normalized strain rate, the normalized wrinkle numbers are similar.

This indicates the normalization method is correct.

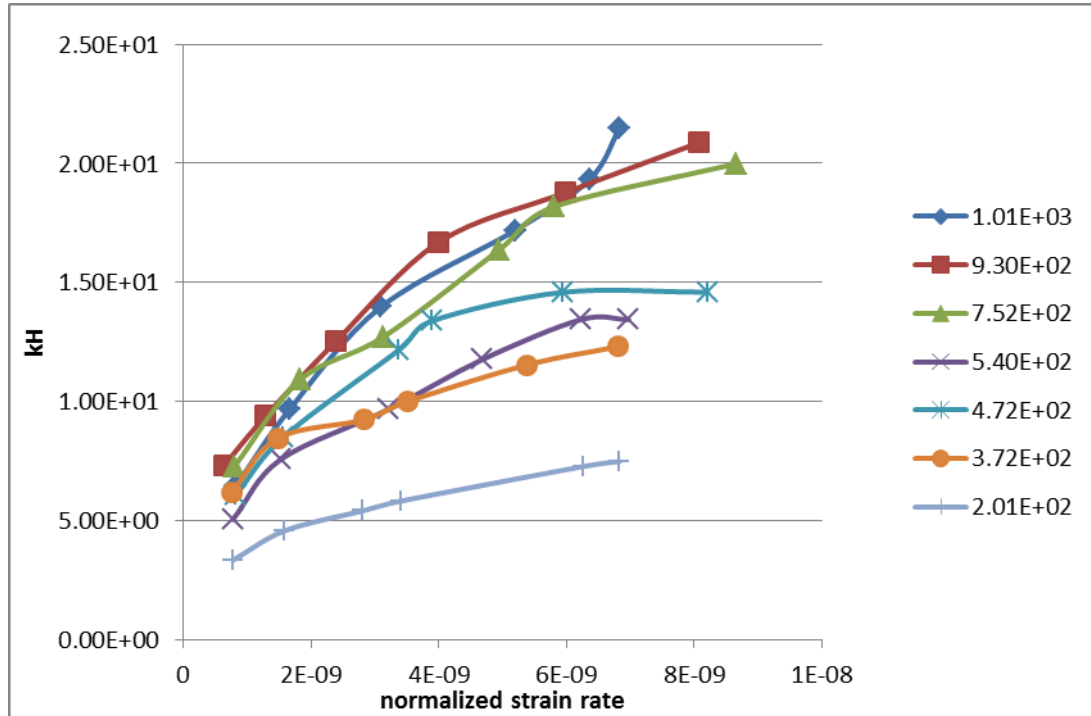


**Figure 31 Normalized wrinkle number  $kh$  versus normalized strain rate.**

Figure 31 shows the quantities of  $kH$  is on order 1 which means the wavelength of wrinkle and the substrate thickness are always comparable. In other words, we do not observe the limiting conditions of either  $\lambda \gg H$  or  $\lambda \ll H$ .

#### 4.4.2 Comparison with theory for films with prestress

According to the relation between the growth rate and wrinkle number derived by Huang and Suo [33] mentioned in chapter 2, we plotted the following figure with various thickness ratios: 2, 5, 10, 15, 20, 25, 540.

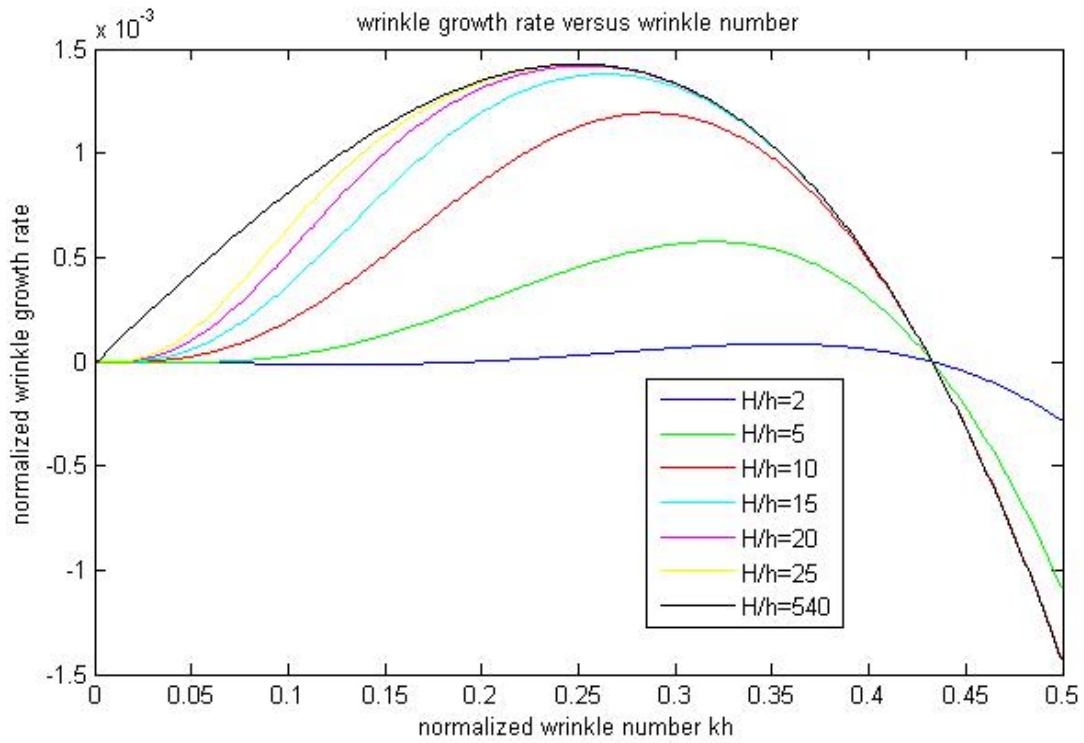


**Figure 32 Normalized wrinkle growth rate versus normalized wrinkle number according to Huang's theory.**

**The pre-strain is -0.012 and the Poisson ratio is 0.3.**

The critical wavenumber above which the wrinkle decays does not change for different thickness ratio according to Figure 32. Besides, each curve has a normalized wrinkle number corresponds to the fastest wrinkle growth rate. It is clear that at large thicknesses, the fastest growing wave number has less dependent on  $H/h$ ; only below  $H/h$  of 15 is there significant dependence. This can be quantified further by plotting the  $k_m \cdot h$  as a function of  $H/h$ .

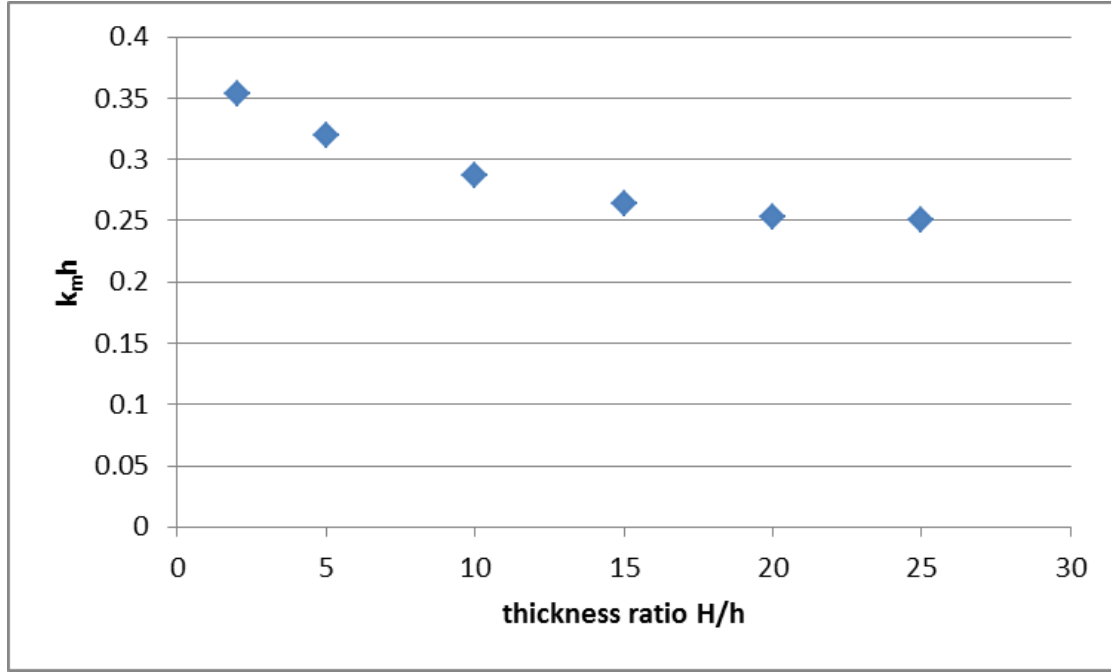


**Figure 33 Fastest growing wave number versus thickness ratio according to Huang and Suo .add citation**  
**The pre-strain is -0.012 and Possion ratio is 0.3.**

From Figure 33, we could see the normalized wrinkle number have a decrease trend with the increase of thickness ratio. However the normalized wrinkle number hardly changes once the thickness ratio  $H/h$  increases above 15.

In our experiment, the number of onset wrinkles is considered to be the fastest growing wavenumber, and the normalized wrinkle number shows a dependence on the substrate thickness even the thickness ratio is much larger than 20 as below.

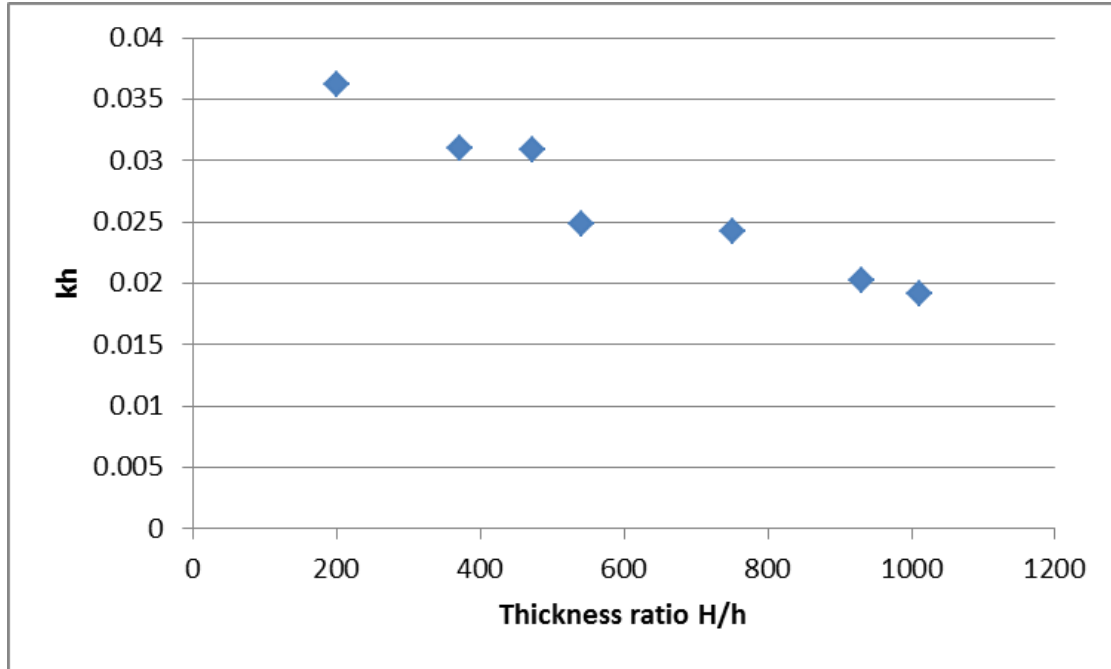


**Figure 34 Measured normalized wrinkle number versus thickness ratio.**  
The strain rate is approximately  $6.0E-09S^{-1}$ .

The difference between our experiments as compared to Huang and Suo's analysis is that for Huang's model, the pre strain (or pre stress) is fixed while in our case, after the strain rate is specified, decrease the substrate thickness will increase the stress in the film which leads to an obvious change in normalized wrinkle numbers. This gives the motivation to estimate the stress as per next section.

#### 4.4.3 Deriving film stress

The goal of this section is to invert Huang's analysis: use the experimental wavelength to estimate the stress experienced by the film. We can calculate (as per equations given by Huang and Suo) the dependence of growth rate on pre strain at a fixed thickness ratio as per Figure 32. This calculation is only done at large  $H/h$  since that is the condition of our experiments.

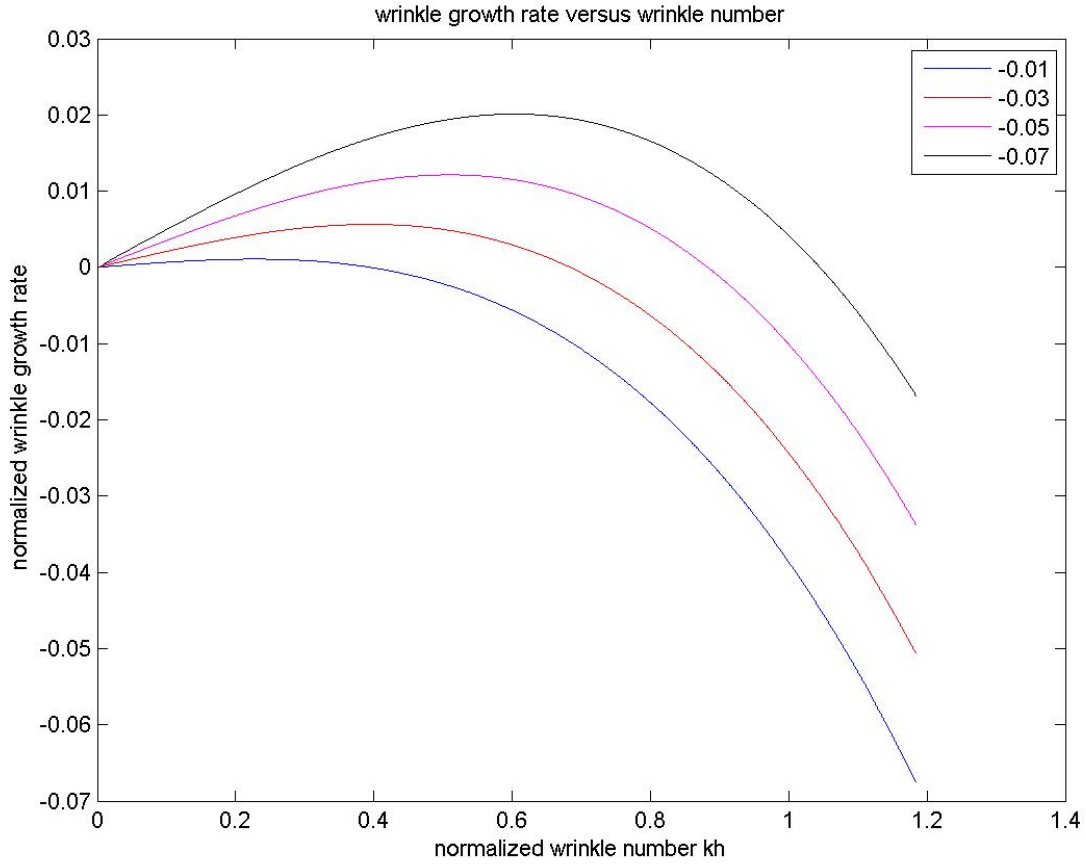


**Figure 35 Normalized growth rate versus normalized wrinkle number in the limit of thickness ratio  $H/h \rightarrow \infty$ . The pre-strain varies.**

From Figure 35, we could see the critical wrinkle number changes under different pre-strain, and the fastest growth rate increases with the increase of pre strain. Moreover, the higher pre strain imported on the film leads to a higher energy in the system, which according to Pocivavsek's analysis[24] will results to a lower wavelength wrinkle. The corresponding dependence of  $k_m \cdot h$  on pre-strain is shown in Figure 36.

In our case, the thickness ratio ranges from 200 to over 1000; in this range Huang's analysis shows no significant dependence of  $k_m h$  on  $H/h$ . We obtained the relation between pre



strain and normalized wrinkle number under Huang's predicating of infinite thickness ratio experiment as showing below.

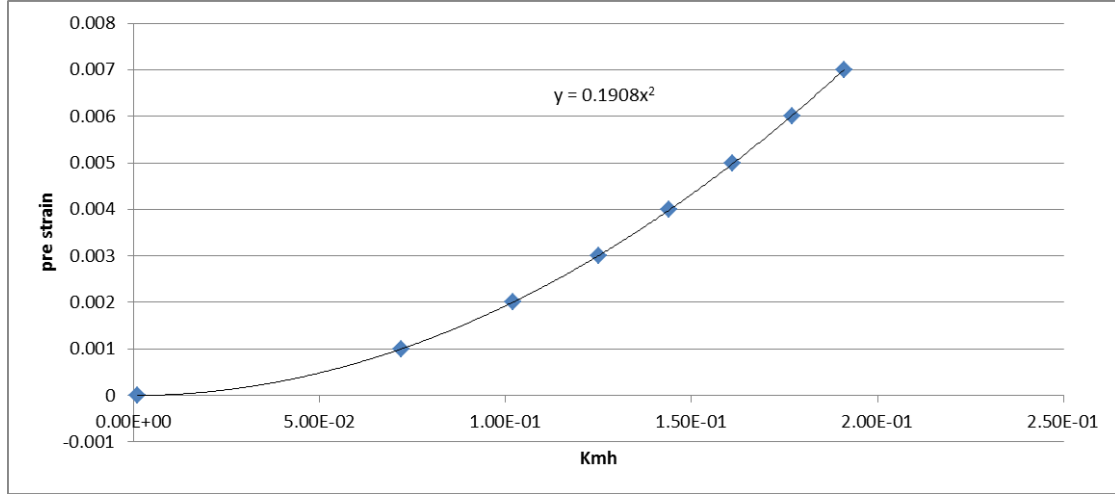


**Figure 36 Pre-strain versus normalized fastest growing wave number, when thickness ratio  $H/h \rightarrow \infty$ .**

The relation obtained from Figure 36 is well-fitted to the expression derived by Sridhar's work as:

$$k_m h = \sqrt{\frac{12\varepsilon_0(1+\nu)}{3}} \quad (16)$$

With given  $\nu=0.3$ ,

$$\varepsilon_0 = \frac{1}{4} \frac{1}{1+\nu} (k_m h)^2 = 0.19(k_m h)^2 \quad (17)$$

We can now use equation 17 to estimate the prestress on the films in our experiments. By substituting the normalized wavenumber  $kh$  obtained from our experiment, we get a value of pre strain. Multiplying this with film modulus, we obtained an estimate stress experienced by film under different thickness ratio, as present in Figure 37.

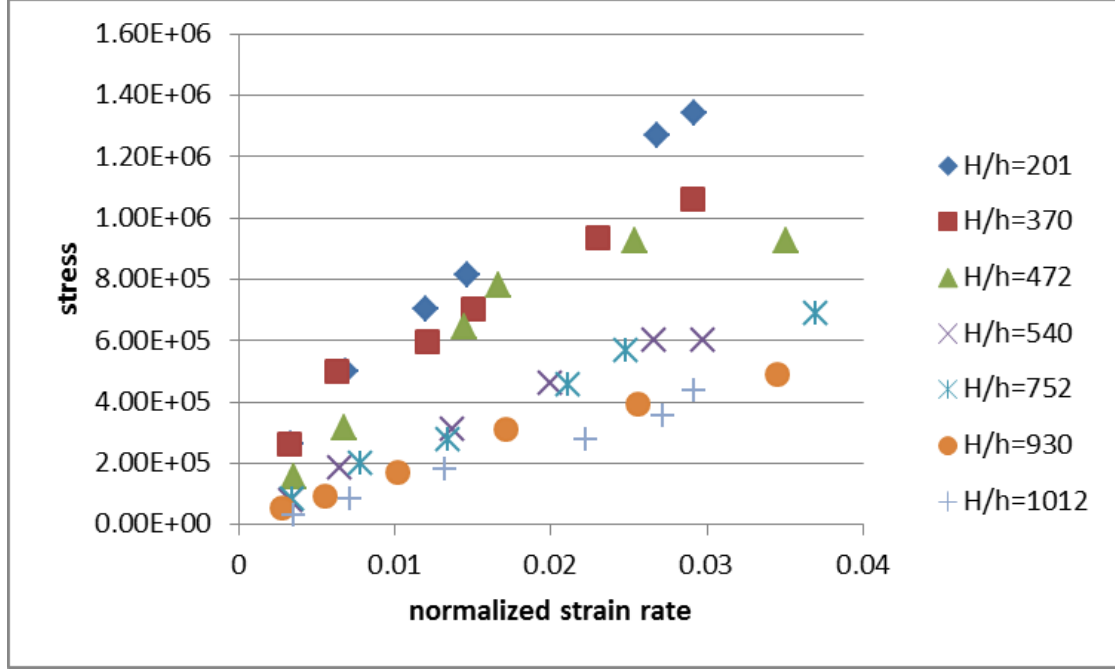


Figure 37 Stress [Pa] on the film versus strain rate  $\dot{\epsilon}$  [ $s^{-1}$ ] for different thickness ratio.

From Figure 37, we find out the stress experienced by film ranges from  $10^4 \sim 10^6$  Pa. however, back to our case, one way to predict the stress might experience by film is to consider the characteristic viscous stress that equals to  $\eta^* \dot{\epsilon}$ , it ranges from 3.5-35 Pa in our case.

Clearly, discrepancies exist in the stress calculated with these two methods. It indicated the film experiences a stress that is many orders of magnitude larger than  $\eta^* \dot{\epsilon}$ . We will therefore consider how such large film stress may be developed.

#### 4.4.4 Relation with strain rate and thickness

First, we compare wavelength  $\lambda$  with film length  $L$ .

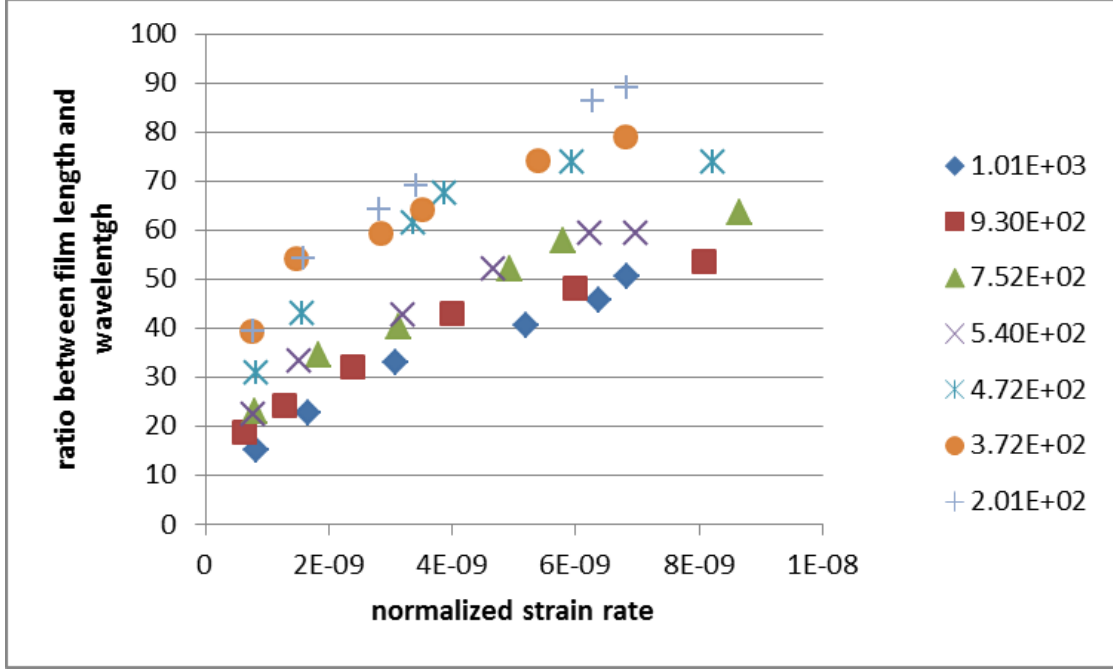


Figure 38 Ratio of film length to wavelength  $L/\lambda$ . The normalized strain rate varies.

From Figure 38, we find that the film length usually exceeds the wavelength by a factor of at least 10, often much higher. Therefore it may be reasonable to treat the film as infinitely long. Thus for the relation derived from the dimensional analysis,

$$kh = f\left(\text{dimensionless rate}, \frac{H}{h}, \frac{L}{h}\right) \quad (18)$$

the last dependence can be ignored. However, the results obtained from this do not seem to agree quantitatively with our experiment data and so later we consider the dependence of the film length  $L$  also.

In the following sections, both cases are considered.

We regarded the thin film in our experiment as a one dimension linear elastic material, applying Euler–Bernoulli beam theory; we get the stress experienced by film as:

$$\sigma = 4\pi^2 \frac{Eh^2}{\lambda^2} \quad (19)$$

Here  $h$  is the thickness of the film,  $\lambda$  is the wavelength of wrinkle,  $E$  is the modulus of the film. In our case, the dimensional analysis suggests one relation as

$$\sigma = \eta \dot{\epsilon} f\left(\frac{\lambda}{H}\right) \quad (20)$$

We assume that the functional form for  $f$  is a power law,

$$\sigma = \eta \dot{\epsilon} \frac{\lambda^n}{H^n} \quad (21)$$

Here,  $\eta$  is the viscosity of substrate and  $\dot{\epsilon}$  is the strain rate in our experiment. Combine equation (19) and (21) to get

$$\lambda = [2\pi]^{2/n+2} h \left[ \frac{E}{\eta \dot{\epsilon}} \right]^{1/n+2} \left[ \frac{H}{h} \right]^{n/n+2} \quad (22)$$

Since  $k=2\pi/\lambda$ , equation (22) gives

$$kh = [2\pi]^{n/n+2} \left[ \frac{\eta \dot{\epsilon}}{E} \right]^{1/n+2} \left[ \frac{H}{h} \right]^{-n/n+2} \quad (23)$$

This suggests that – if the functional form  $f$  is indeed a power law in  $H/h$  – then the dependence of  $kh$  on rate and the dependence of  $kh$  on  $H$  are related to each other through the common parameter  $n$ . To test this idea, we rearrange the above equation into log form to obtain

$$\log(kh) = \frac{-n}{n+2} \log\left(\frac{H}{2\pi h}\right) + \frac{1}{n+2} \log\left(\frac{\eta \dot{\epsilon}}{E}\right) \quad (24)$$

This equation is in the form of  $y=b+aX$ . Fitting the  $kh$  versus rate data measured at a single value of  $H/h$  allows the slope  $a=1/(n+2)$  to be determined; we can then plot the intercept values  $b$  against  $\log(H/h)$  to and test if the corresponding slope is  $-n/(n+2)$ .

Figure 39 plotted the data of Figure 29 in log-log form. In this plot, cases with less than 5 wrinkles were visible (corresponding to points with  $kh < 1.35 \times 10^{-2}$ ) have been ignored since the corresponding “counting error” on the y-axis is too large. Fits of equation 24 to the  $\log(kh)$

versus  $\log(\text{rate})$  data are shown in Figure 39. The corresponding values of slope are shown in Table 4.

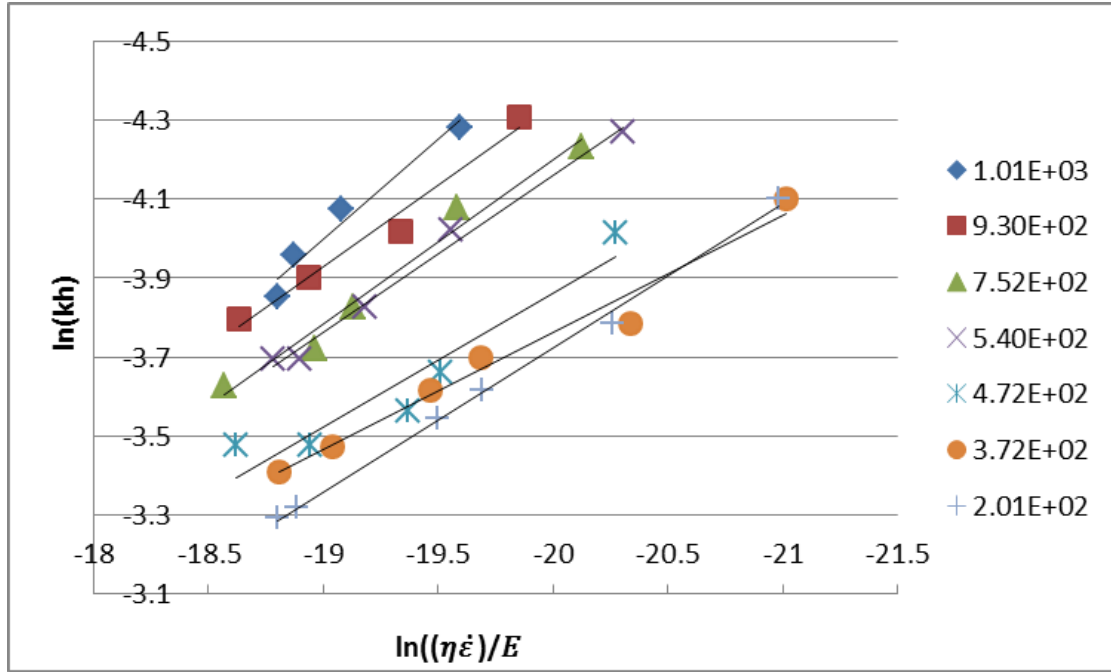


Figure 39 Logarithm of normalized wrinkle number versus logarithm of normalized strain rate.

**Table 4 Logarithm of normalized wrinkle number versus logarithm of normalized strain.**

H/h	L/H	slope	intercept
201	0.0746	0.2968	2.1735
372	0.0403	0.365	3.5751
472	0.0318	0.3383	2.9039
540	0.0278	0.3976	3.7905
752	0.0199	0.4163	4.1246
930	0.0161	0.4127	3.9133
1012	0.0148	0.5035	5.5678

From Table 4, we find that the slopes range from 0.3 to 0.5. Since we are assuming that the film is infinite in length, this analysis is best suited for large L/H values; in these cases, the values are range between 0.3 and 0.4. Somewhat arbitrarily, we will assign a common value of 1/3 to the slope; in that case  $n=1$  so  $-n/(n+2)= -1/3$ . Thus, this analysis predicts that the dependence of  $kh$  on  $H/h$  is a power law with exponent -0.33.

To test this, the fitting analysis leading to Table 1 was repeated by fixing the value of slope to 1/3 for all thickness ratios. The corresponding fits and values of intercept are shown in Figure 40.

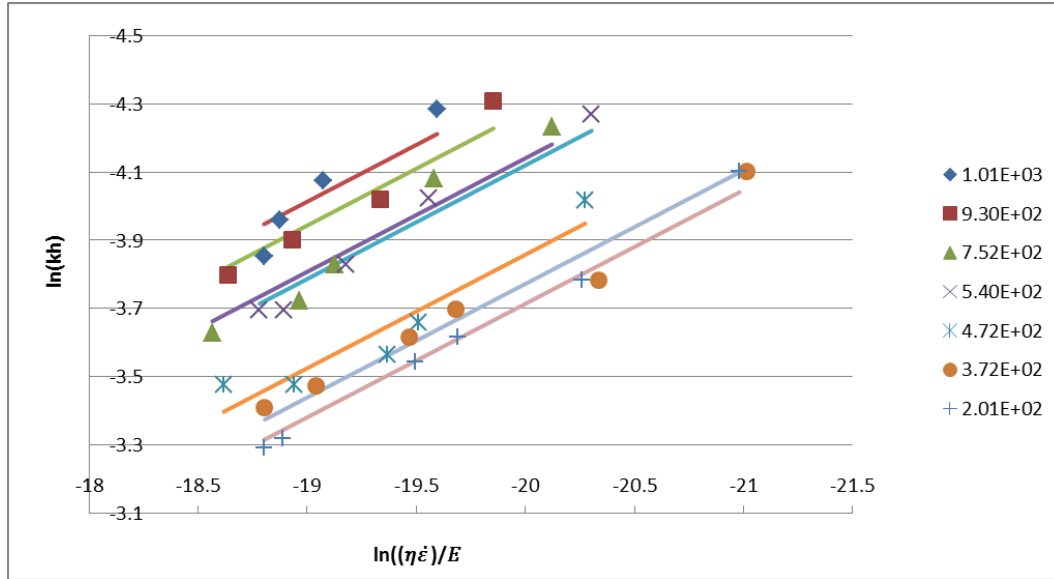


**Figure 40 Fitted normalized wrinkle number versus normalized strain rate, with their correspondently fitting line that fixed the slope to  $\frac{1}{3}$ .**

**Table 5 Fitted normalized wrinkle number versus normalized strain rate, slope fixed to  $\frac{1}{3}$ .**

H/h	Slope	intercept
201	$\frac{1}{3}$	2.3198
372	$\frac{1}{3}$	2.3897
472	$\frac{1}{3}$	2.5256
540	$\frac{1}{3}$	2.5465
752	$\frac{1}{3}$	2.8085
930	$\frac{1}{3}$	2.8942
1012	$\frac{1}{3}$	2.9525

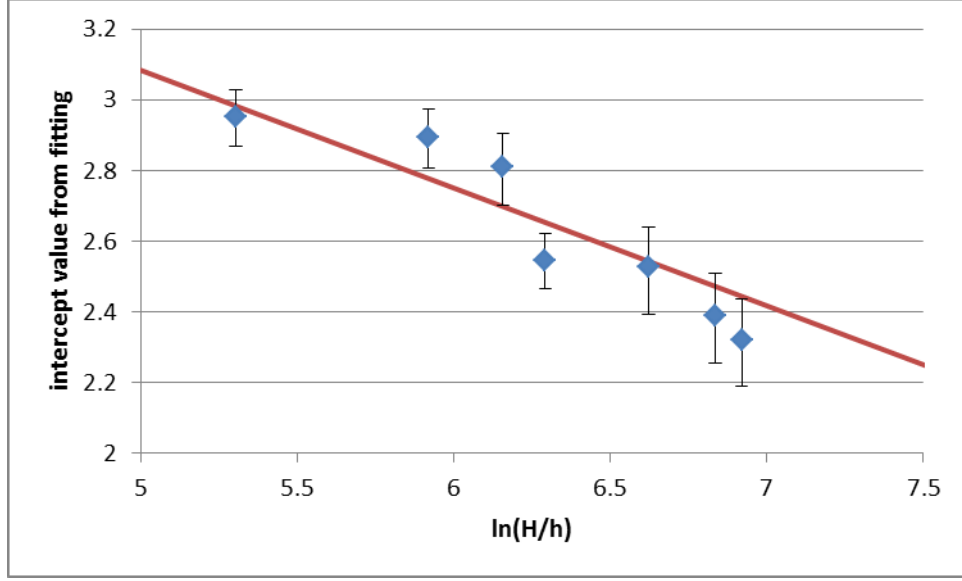


**Figure 41 Intercept versus logarithm of thickness ratio.**  
The red line is not a fit, it is simply a linear line with slop of  $\frac{1}{3}$

The blue diamonds are the intercept of the linear equation from fitting the experiment result while fixing the slope to  $\frac{1}{3}$ . Via considering the error in the wrinkle number counting process, we get the minimum and maximum wrinkle number, fitting them with equation 24, we obtained the minimum intercept and the maximum intercept. The error bar of Figure 41 is estimated from this method.



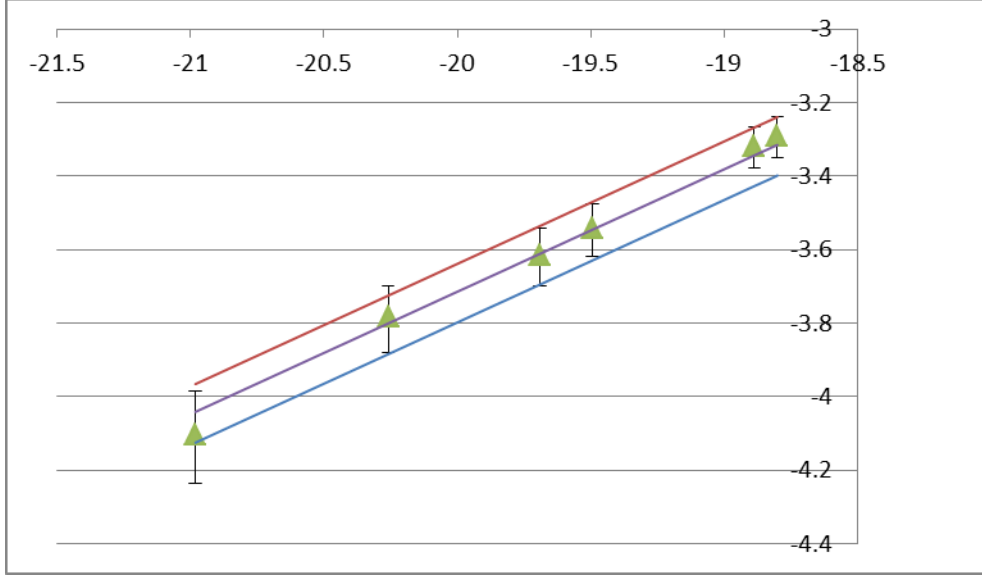


**Figure 42** An example of obtaining error bar of a single thickness ratio for figure 41

The red line is a fitting with the maximum wavenumber and the blue line is a fitting with the minimum wavenumber. The triangle is the experiment data and the purple line is its fitting. Intercept of red line and blue one indicate the error bar for a single point in Figure 41.

A plot of the intercept of the fitting lines versus  $\ln(H/h)$  is shown in Figure 41 along with a line of slope  $-1/3$ . A reasonable agreement is found, i.e. the basic idea inherent in equation 21 is not contradicted. Accordingly, equation 21 (with  $n=1$ ) becomes

$$\sigma = \eta \dot{\epsilon} \frac{\lambda}{H} \quad (25)$$

However, even though the  $H$ -dependence and rate dependence predicted by this equation is not too far from what is seen experimentally, quantitatively, this equation is not in agreement with the stresses: the stress obtained from equation 25 ranges from 3-30 Pa which is far lower than the stress in the film which is calculated in the last section. So even the dependence of wavelength and substrate thickness on stress is reasonable, we are still not able to obtain the absolute values quantitatively.

It is therefore useful to reconsider the dependence of viscous stress on the length of the film, i.e. the film length is considered as infinite and thus its effect could not be neglected.

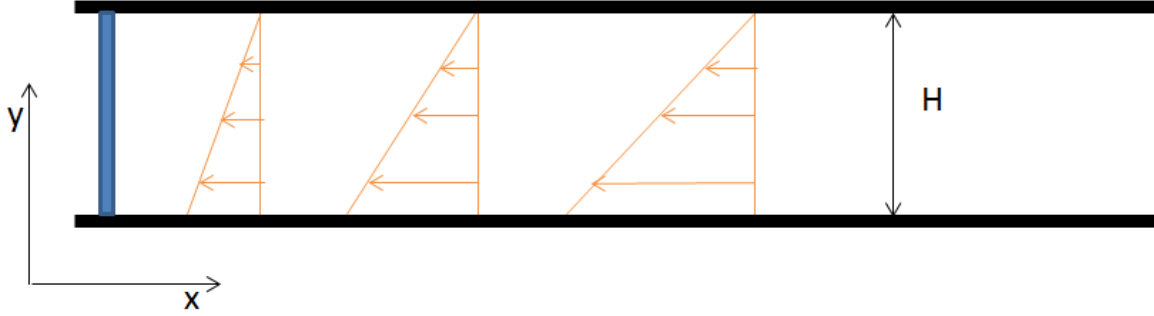


**Figure 43 Velocity profile in the substrate prior to buckling.**

The blue column indicates the center of film, H is the height of the substrate, consider the substrate as Newtonian fluid.

$$\tau = \eta \frac{dv}{dy} \quad (26)$$

Where  $\tau$  is the shear stress and  $v$  is the velocity and  $\eta$  is the viscosity of substrate. The velocity profile along the bottom surface is

$$v_{x0} = -\dot{\epsilon}x \quad (27)$$

Where  $\dot{\epsilon}$  is the strain rate and  $x$  is the distance away from center. So the shear stress on the top surface of the substrate would be:

$$\tau = \eta \frac{\dot{\epsilon}x}{H} \quad (28)$$

Since the compressive stress on the film is provided by shear stress, We obtained

$$\eta \frac{\dot{\epsilon}x}{H} = h \frac{d\sigma_{film}}{dx} \quad (29)$$

Where  $\sigma_{film}$  is the stress on the top of substrate.  $h$  is the film thickness. Integrating the above equation, we have

$$\sigma_{film} = \frac{\eta \dot{\epsilon}}{Hh} \int_0^{L/2} x dx = \frac{\eta \dot{\epsilon}}{Hh} \frac{L^2}{8} \quad (30)$$

Where  $L$  is the length of the film. Use the dimensionless method, we get an expression as: Replace the lowercase  $l$  with  $L$  in the equations below

$$\sigma_{film} = \frac{\eta \dot{\epsilon}}{Hh} \frac{L^2}{8} = 4\pi^2 \frac{Eh^2}{\lambda^2} \quad (31)$$

Rearrange the above equation, substitute  $k=2\pi/\lambda$ , to get

$$kh = \left(\frac{1}{8}\right)^{1/2} \frac{L}{h} \left(\frac{\epsilon \dot{\eta}}{E}\right)^{1/2} \left(\frac{H}{h}\right)^{-1/2} \quad (32)$$

Rearrange the above equation into log form we obtained

$$\log(kh) = \frac{-1}{2} \log\left(\frac{8hH}{L^2}\right) + \frac{1}{2} \log\left(\frac{\eta \dot{\epsilon}}{E}\right) \quad (33)$$

This suggests that  $kh$  depends on strain rate and on  $H$  with a  $1/2$  power law. Indeed Table 4 showed that relatively small values of  $L/H$ , the slope of 0.5 are approached. Thus we redid the fitting analysis of Table 5 by fixing the value of slope to 0.5 at all thickness ratios. The corresponding fits are shown in Figure 43 and the intercepts are plotted as a function of  $\log(H/h)$  in Figure 43.

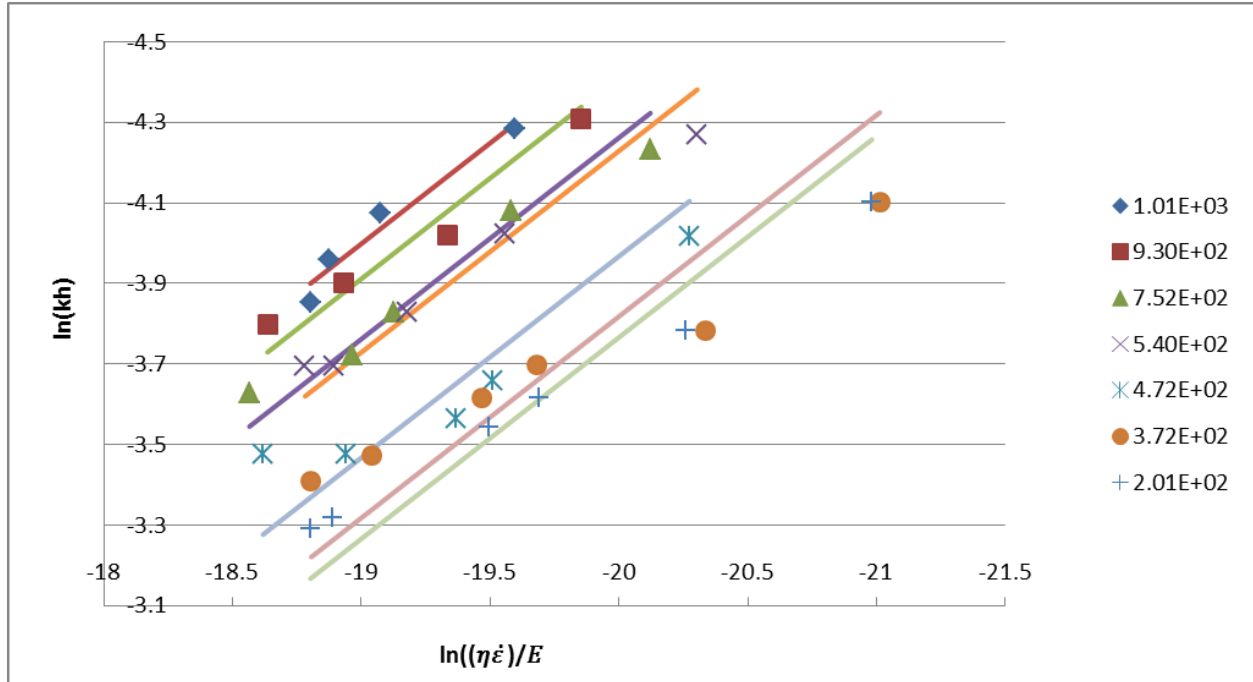
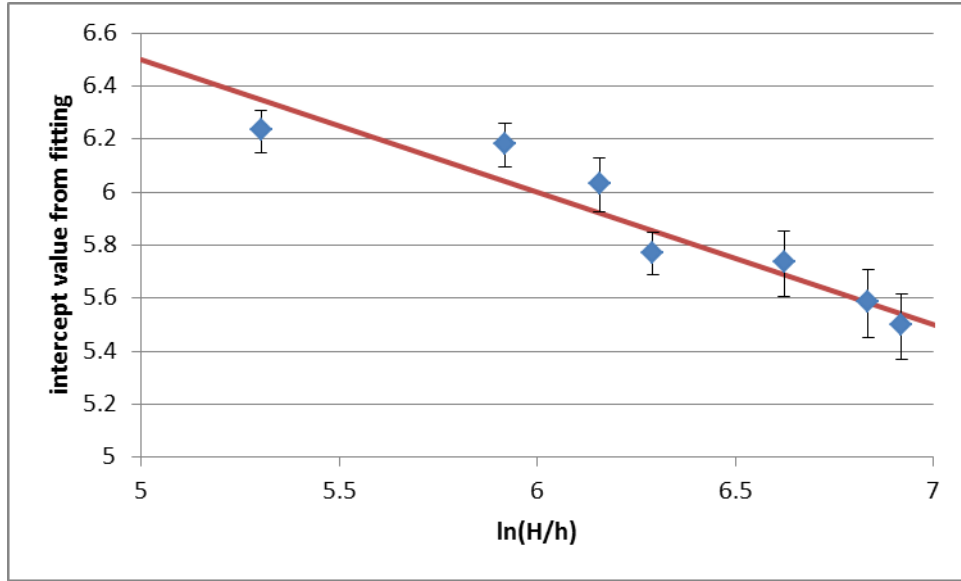


Figure 44 Fitted normalized wrinkle number versus normalized strain rate, slope fixed to  $\frac{1}{2}$ , with their correspondently fitting line that fixed the slope to  $\frac{1}{2}$ .

Table 6 Fitted normalized wrinkle number versus normalized strain rate, slope fixed to  $\frac{1}{2}$ .

H/h	Slope	Intercept
201	0.5	6.2335
372	0.5	6.1815
472	0.5	6.0320
540	0.5	5.7705
752	0.5	5.7375
930	0.5	5.5880
1012	0.5	5.5008



**Figure 45 Intercept versus log nature of thickness ratio.**  
The red line is not a fit, it is simply a linear line with slop of  $\frac{1}{2}$

A plot of the intercept of the fitting lines versus  $\ln(H/h)$  is shown in Figure45 The error bar is estimated same as the Figure 41. A reasonable agreement is found, i.e. the basic idea inherent in equation 33 is not contradicted. We calculated the stress according to equation33 compared them with the data calculated by Huang's theory

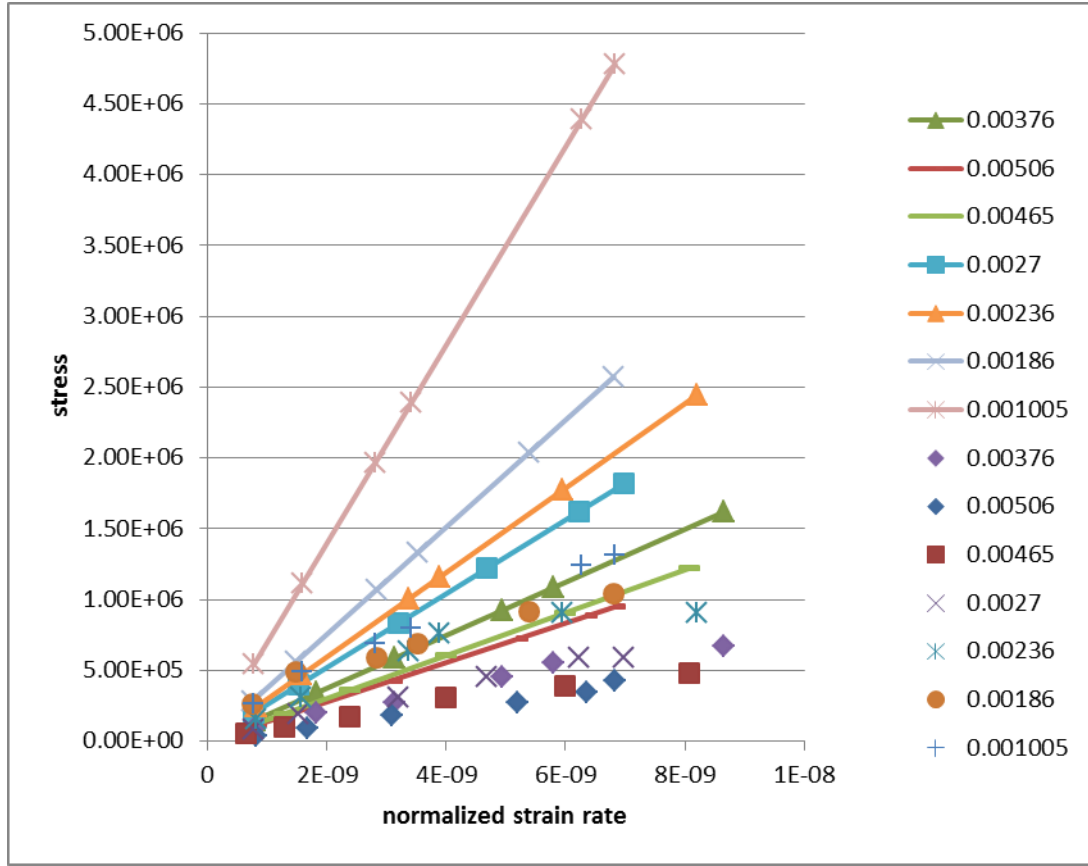


**Figure 46 Stress versus normalized strain rate under different substrate thickness**  
The markers with smooth lines are the data calculated by equation 31 and the other type of scatter pattern are data calculated by Huang's theory. The right legend indicate the substrate thickness[m]

From Figure 46, we found the stress calculated by equation 31 has the similar order compared with the stress measured by Huang's work.

## 5.0 CONCLUSION AND FUTURE WORK

### 5.1 CONCLUSION

In this study, we developed a method to generate dynamical wrinkles on the films placed at the interface between air and a viscous polymer. A method of measuring the substrate thickness without the interference of edge effect has been developed. The wrinkle number and the critical strain of onset of wrinkles are obtained by processing the recorded video of the compression.

A relation among the wrinkle number the compressed strain rate and the thickness ratio has been revealed by analyzing the normalized wrinkle behavior under controlled substrate thickness and compressing strain rate. We described the dependence of the wrinkle number on the strain rate and the thickness ratio with a power law expression. In the limit of infinite film length and thin substrate, the experimental data are consistent with a power index of strain rate is  $\frac{1}{3}$  and the power index of thickness ratio is  $-\frac{1}{3}$ . However, if the length of the film is regarded as finite, the power indices of  $\frac{1}{2}$  and  $-\frac{1}{2}$  seem more suitable.

The wrinkle number normalized with the substrate thickness is small in our project. However, this may be no longer the case while the film is in nano-scale. For liquid/liquid system, similar wrinkle behavior could be observed if the substrate thickness is big and low or comparable viscosity. Otherwise, people may not observe the same wrinkle behavior.

## 5.2 FUTURE WORK

First, we recommend studying the discrepancy between the stress predicted in Huang's model and one measured in our experiment.

We suggest studying the effects of altering the material used in the viscous substrate and lowering the substrate thickness with the experimental method developed in this thesis. This further work will help to establish a method to measure the modulus from the wrinkle number the film thickness.

Furthermore, in order to develop a more practical way of measuring the nano-scale polymeric films, we suggest investigate the application of the method on polymeric films formed via interfacial-group-coupling between two immiscible polymer bulks.



## **APPENDIX A**

### **STUDY OF POLYMERIC FILMS FORMED BY INTERFACIAL REACTIVE COUPLING**

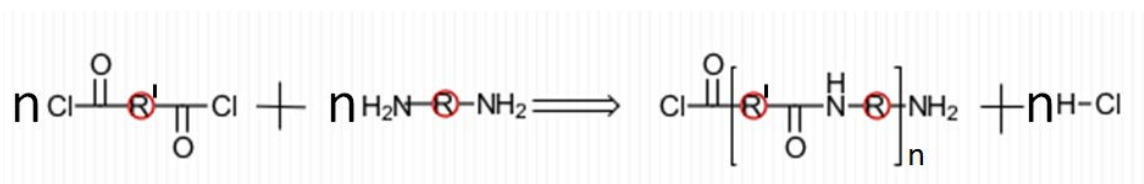
As mentioned in the previous chapters, the main task of this project is to derive a measurement to characterize the properties of interfacial film. In this chapter, a formation of film via polymerization has been studied.

The main goal of this experiment is to generate a film in the interface between two immiscible bulks by reactive coupling reaction, deform the film to induce wrinkle pattern which could be used to characterize the film properties. The original goal of this M.S. project was to develop a buckling method to characterize the mechanical properties of this film. However, as will be demonstrated in this Appendix, the experimental system chosen was found ill-suited for this purpose.

## A.1 SELECTING REACTANTS

Our interest was in producing thin polymer films at the interface in oil/water system. The general idea was to synthesize a film from the reaction between two functional species, each dissolved in a different phase, arriving at the interface and forming a film by chemical reaction.

The reaction selected for this is a variation of the nylon rope trick[34] in which an oil phase containing diacid chloride is contacted with a diamine dissolved in water. The general reaction at the interface is.:





This is an interfacial step-growth polymerization, leading to the formation of a polyamide film. It is often called the nylon rope trick since it is possible to pick up the film with tweezers continuously; as the polymer is removed from the interface, new polymer is continuously formed by continued reaction. A molecule of hydrogen chloride is given off and the condensation polymer is formed.

Holmes and Crosby generated wrinkle on films floating on water via lifting the film from center bottom with a round probe[10]. We attempted similar method and induce wrinkle in the hope of correlating the wrinkle patterns to film properties like thickness and modulus. In order to reach this goal, the film has to be thin enough to form wrinkle as well as possess good mechanical properties otherwise it will tear.

In order to get a film with sufficient robustness to be handled easily, relative high molecular weight chemicals with the above functional groups were considered to be appropriate

reactants. Teraphthaloyl chloride and branched polyethyleneimine (PEI) are selected as reactants in this case. Since PEI is multifunctional, the films are cross linked.

**Table 7 Properties of the reactant selected for synthesizing polymeric film.**

Chemicals	Density (g·cm <sup>3</sup> )	Melting point (°C)	Molweight (g/mol)	Structure
teraphthalo-yl chloride	1340	83	203	
PEI	1030	60	25000	

\*n is 53 for the given molecular weight PEI in our case

## A.2 CALCULATING AMOUNTS OF REACTANTS

In order to have a general ideal of the reactants usage, first, we consider of terephthaloyl chloride as the limit reactant and assume it is fully reacted during the polymerization, two limit cases are considered. i.e one mole of PEI would react with  $53 \times 2 + 1 = 107$  mole terephthaloyl chloride, or one mole terephthaloyl chloride reacts with two mole PEI. With this assumption we had an approximate relation between the film thickness we want to obtained and the amount of terephthaloyl chloride we should add into the beaker (we neglected the swelling effect of the final product in the water solution).

$$\frac{S \times h \times \rho}{M_w} \times M_{tc} = m_{tc} \quad (34)$$

Where S is the surface area of beaker, h is the thickness of the film;  $\rho$  is the density of the film which is assumed to be  $1.0\text{g/cm}^3$ . Mw is the unit molecular weight of the final products which is  $38910\text{-}50132\text{g/mol}$ .  $M_{tc}$  indicates the molecular weight of terephthaloyl chloride,  $m_{tc}$  is the mass of terephthaloyl chloride.

### **A.3 FILM SYNTHESIS**

0.0032 grams of teraphthaloyl-chloride were dissolved into 200 ml mineral oil, and designated solution A. 0.1125 g PEI were placed in 100 ml distilled water, and designated as solution B. 20 ml solution B, was poured into a standard 50ml beaker, and a 2 mm thick layer of mineral oil was poured on it. Then 5 ml of solution A was dispensed gently and uniformly on top of the oil with a pipette. The beaker was covered with a cap, and let stand for 12 hours. A micro scale thickness film formed in the interface.

### **A.4 EXPERIMENTAL METHODS**

The key idea of this experiment is to deform the interface and forces it to buckle and form wrinkles. In this project, three methods have been considered.

The first method is to put a drop of water on the film surface. This mimic the experiments of Huang et.al [25] Radial wrinkles appear under the capillary force of the droplet. The second method is to place a disk on the film surface. Wrinkle will be introduced by the weight of the disk. This approach was followed by both Huang as well as Cerda [35]. The third method is poking the film with a round end wire, similar to the approach of Holmes and Crosby[10]. For the first two methods, it is difficult to apply a continuous force on the film. In contrary, force that introduced on the film could be controlled precisely by adjusting the displacement of the beaker on the platform in the third method.

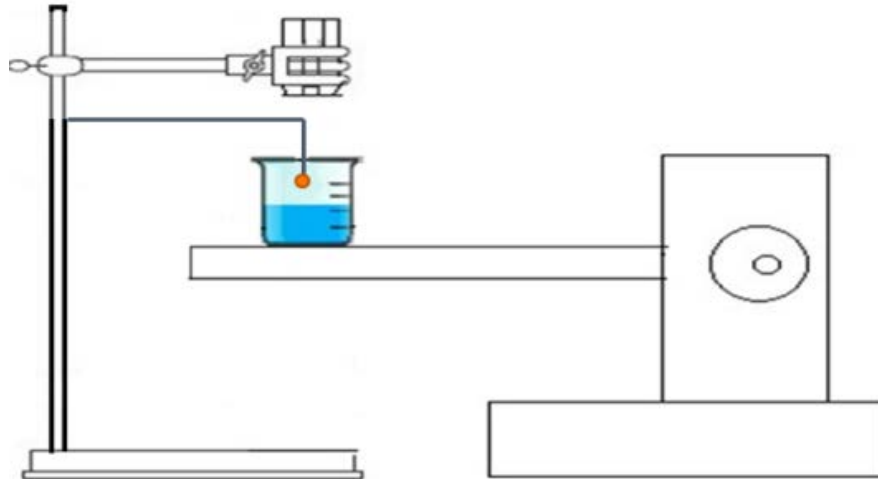


**Figure 47 Setup of the poking experiment.**

Beaker is placed on a height-adjustable platform. A bent wire with a round end is fixed on a metal stand so that the round end can poke the film. A camera mounts above the beaker.

## A.5 RESULTS

The first method does not work out very well, placing droplet did not induced obviously wrinkle. However wrinkle formed via placing a disk in the top center of the film as well as poking it with a round end wire.

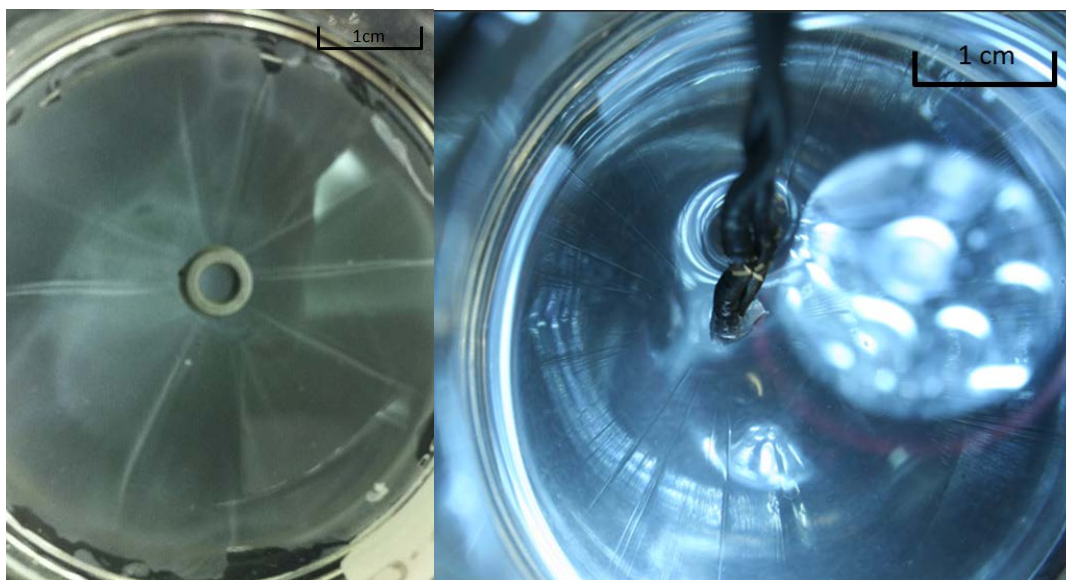


**Figure 48 Wrinkles induction on the interfacial film.**

**Left: by placing a disc on the center.**

**Right: by poking at the center.**

Thus, we were able to generate wrinkles on interfacial-generated films. Repeated experiments however showed significant irreproducibility. As we carried out the step of generating films in petridish at same condition, different surface phenomena have been observed during the film formation process.

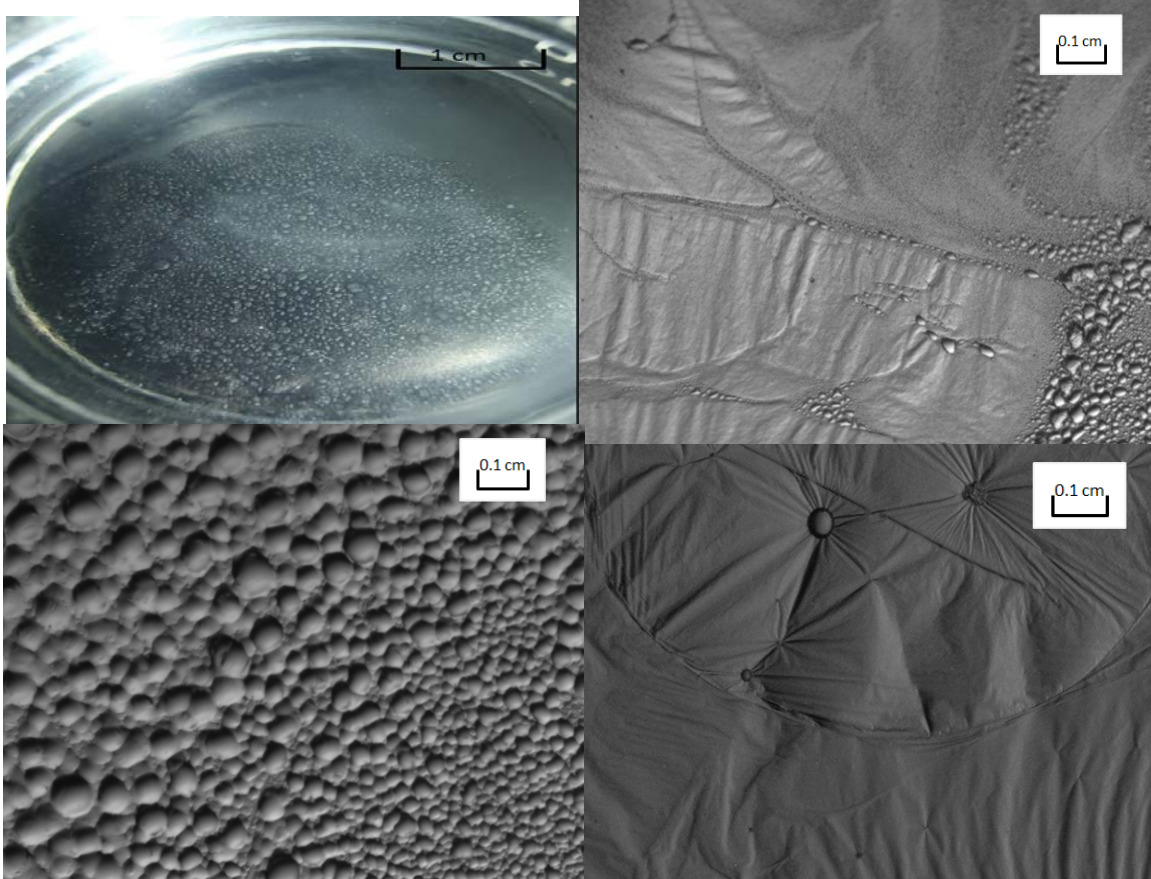


**Figure 49 Images of spherical formations near the film surface.**

The top left image is taken by camera other images are taken from microscope. From image 49, spherical formations are seen in the film surface.

We also noticed self-wrinkling happened sometimes during film generation; we capture the image of films under camera and digital microscope and get the Figure 50.

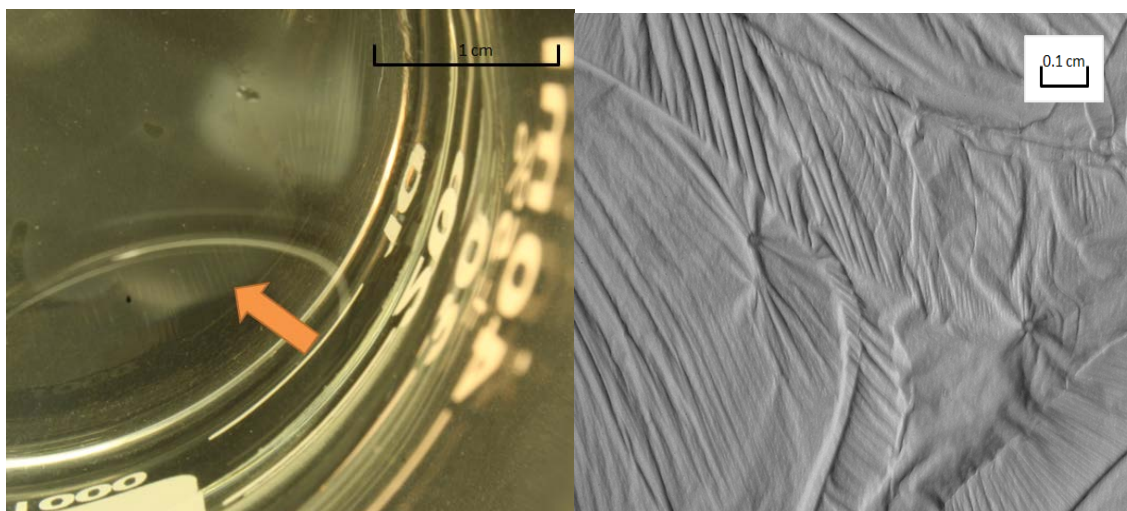


**Figure 50 Images of film surface.**

From Figure 49 and 50, we found film generated with the mentioned method have a trend of self-wrinkling and have less reproducibility and consistent for further study. So we did not adopted this film as our experiment sample, instead, we developed a new experiment method which could induce dynamic wrinkle pattern and used 5micrometer thick clear polyester Mylar film for further study.



## BIBLIOGRAPHY

1. Cerda, E. and L. Mahadevan, *Geometry and physics of wrinkling*. Physical Review Letters, 2003. **90**(7).
2. Stafford, C.M., et al., *A buckling-based metrology for measuring the elastic moduli of polymeric thin films*. Nature Materials, 2004. **3**(8): p. 545-550.
3. Bowden, N., et al., *The controlled formation of ordered, sinusoidal structures by plasma oxidation of an elastomeric polymer*. Applied Physics Letters, 1999. **75**(17): p. 2557-2559.
4. Vella, D., et al., *The macroscopic delamination of thin films from elastic substrates*. Proceedings of the National Academy of Sciences of the United States of America, 2009. **106**(27): p. 10901-10906.
5. Liang, J., et al., *Relaxation of compressed elastic islands on a viscous layer*. Acta Materialia, 2002. **50**(11): p. 2933-2944.
6. Okayasu, T., et al., *Spontaneous formation of ordered lateral patterns in polymer thin-film structures*. Advanced Functional Materials, 2004. **14**(11): p. 1081-1088.
7. Chung, J.Y., A.J. Nolte, and C.M. Stafford, *Surface Wrinkling: A Versatile Platform for Measuring Thin-Film Properties*. Advanced Materials, 2011. **23**(3): p. 349-368.
8. Ventsel, E. and T. Krauthammer, *Thin plates and shells : theory, analysis, and applications* 2001, New York: Marcel Dekker. xiv, 666 p.
9. Jiang, H.Q. and J.P. Zhang, *Mechanics of Microtubule Buckling Supported by Cytoplasm*. Journal of Applied Mechanics-Transactions of the Asme, 2008. **75**(6).
10. Holmes, D.P. and A.J. Crosby, *Draping Films: A Wrinkle to Fold Transition*. Physical Review Letters, 2010. **105**(3).
11. Lin, P.C. and S. Yang, *Spontaneous formation of one-dimensional ripples in transit to highly ordered two-dimensional herringbone structures through sequential and unequal biaxial mechanical stretching*. Applied Physics Letters, 2007. **90**(24).

12. Tolpygo, V.K. and D.R. Clarke, *Surface rumpling of a (Ni, Pt)Al bond coat induced by cyclic oxidation*. Acta Materialia, 2000. **48**(13): p. 3283-3293.
13. Tolpygo, V.K. and D.R. Clarke, *Wrinkling of alpha-alumina films grown by oxidation - II. Oxide separation and failure*. Acta Materialia, 1998. **46**(14): p. 5167-5174.
14. Tolpygo, V.K. and D.R. Clarke, *Wrinkling of alpha-alumina films grown by thermal oxidation - I. Quantitative studies on single crystals of Fe-Cr-Al alloy*. Acta Materialia, 1998. **46**(14): p. 5153-5166.
15. Volynskii, A.L., et al., *Mechanical buckling instability of thin coatings deposited on soft polymer substrates*. Journal of Materials Science, 2000. **35**(3): p. 547-554.
16. Bull, S.J. and L.J. Balk, *Adhesion and delamination of interfaces*. Journal of Physics D-Applied Physics, 2011. **44**(3).
17. Huang, H., et al., *Characterizing polymer brushes via surface wrinkling*. Chemistry of Materials, 2007. **19**(26): p. 6555-6560.
18. Jiang, X.Y., et al., *Controlling mammalian cell spreading and cytoskeletal arrangement with conveniently fabricated continuous wavy features on poly(dimethylsiloxane)*. Langmuir, 2002. **18**(8): p. 3273-3280.
19. Chan, E.P., et al., *Quantifying the Stress Relaxation Modulus of Polymer Thin Films via Thermal Wrinkling*. Acs Applied Materials & Interfaces, 2011. **3**(2): p. 331-338.
20. Chung, J.Y., et al., *Stiffness, Strength, and Ductility of Nanoscale Thin Films and Membranes: A Combined Wrinkling-Cracking Methodology*. Nano Letters, 2011. **11**(8): p. 3361-3365.
21. Cerda, E., K. Ravi-Chandar, and L. Mahadevan, *Thin films - Wrinkling of an elastic sheet under tension*. Nature, 2002. **419**(6907): p. 579-580.
22. Biot, M.A., *Folding Instability of a Layered Viscoelastic Medium under Compression*. Proceedings of the Royal Society of London Series a-Mathematical and Physical Sciences, 1957. **242**(1231): p. 444-454.
23. Bourdieu, L., et al., *Buckling of Polymerized Monomolecular Films*. Physical Review Letters, 1994. **72**(10): p. 1502-1505.
24. Pocivavsek, L., et al., *Stress and fold localization in thin elastic membranes*. Science, 2008. **320**(5878): p. 912-916.
25. Huang, J., et al., *Capillary wrinkling of floating thin polymer films*. Science, 2007. **317**(5838): p. 650-653.
26. Cerda, E., *Mechanics of scars*. Journal of Biomechanics, 2005. **38**(8): p. 1598-1603.

27. Geminard, J.C., R. Bernal, and F. Melo, *Wrinkle formations in axi-symmetrically stretched membranes*. European Physical Journal E, 2004. **15**(2): p. 117-126.
28. Chung, J.Y., A.J. Nolte, and C.M. Stafford, *Diffusion-Controlled, Self-Organized Growth of Symmetric Wrinkling Patterns*. Advanced Materials, 2009. **21**(13): p. 1358-1362.
29. Chung, J.Y., et al., *Quantifying Residual Stress in Nanoscale Thin Polymer Films via Surface Wrinkling*. Acs Nano, 2009. **3**(4): p. 844-852.
30. Huang, R., *Kinetic wrinkling of an elastic film on a viscoelastic substrate*. Journal of the Mechanics and Physics of Solids, 2005. **53**(1): p. 63-89.
31. Huang, R. and Z. Suo, *Wrinkling of a compressed elastic film on a viscous layer*. Journal of Applied Physics, 2002. **91**(3): p. 1135-1142.
32. Sridhar, N., D.J. Srolovitz, and Z. Suo, *Kinetics of buckling of a compressed film on a viscous substrate*. Applied Physics Letters, 2001. **78**(17): p. 2482-2484.
33. Huang, R. and Z. Suo, *Instability of a compressed elastic film on a viscous layer*. International Journal of Solids and Structures, 2002. **39**(7): p. 1791-1802.
34. PaulW.Morgan, *The Nylon Rope Trick Demonstration of condensation polymerization*. journal of Chemical Education, 1959. **36**.
35. Vella, D., M. Adda-Bedia, and E. Cerda, *Capillary wrinkling of elastic membranes*. Soft Matter, 2010. **6**(22): p. 5778-5782.